Effects of Friction on a Localized Structure in a Baroclinic Current

HUMIO MITSUDERA

CSIRO, Division of Atmospheric Research, Mordialloc, Victoria, Australia

ROGER GRIMSHAW

Department of Mathematics, Monash University, Clayton, Victoria, Australia

(Manuscript received 21 July 1992, in final form 1 December 1992)

ABSTRACT

In this paper, the effects of bottom and interfacial friction on *localized* baroclinic instability are discussed in the weakly nonlinear, long-wave limit. Using a quasigeostrophic two-layer model in which the lower layer is assumed to be deep, we have derived a coupled evolution equation set that consists of a KdV-type equation for the upper layer and a linear long-wave equation for the lower layer. A perturbation theory reveals that there are multiple equilibria in this system, where baroclinic energy conversion and frictional dissipation are in balance; the flow is not forced externally, and multiplicity here refers to the presence or absence of solitary waves propagating steadily on a zonal flow. Further, direct numerical calculations show a rich variety of behavior of solitary waves, including steady, periodic, and complicated interacting evolutions. For a two-layer model to have multiple steady or oscillatory states, both bottom and interfacial friction should be included because if one of these vanishes, friction destabilizes rather than damps the otherwise neutral waves. The localized baroclinic instability is highly suggestive of the dynamics of the Kuroshio large meander.

1. Introduction

Coherent and localized structures in atmospheric and oceanic currents, such as atmospheric blocking and large oceanic meanders, have a significant impact on regional climate and fisheries because they persist beyond the periods associated with synoptic-scale variability. It has been pointed out that baroclinic processes are important for some of these localized phenomena. An example, which is associated with the ocean, is the formation of the Kuroshio large meander. It is well known that the Kuroshio current shows bimodality in its path, which is either a straight path or a large meander. Both of these paths can persist stably for a few years off the southwest coast of Japan, but transitions occur rather quickly (within a few months). In a numerical experiment with a two-layer model, Yoon and Yasuda (1987) have shown that there are multiple equilibria, and the transition occurs through baroclinic processes rather than barotropic processes. Further, they have shown that a solitary disturbance develops into a large meander only when the initial disturbance is large enough. As for atmospheric blocking phenomena, observations have pointed out that baroclinic processes are important for the formation stage through the local interaction between a synoptic-scale cyclone and a planetary-scale wave (e.g., Nakamura and Wallace 1990), and even for the fully developed stage in some cases (e.g., Hartman and Ghan 1980; Mak 1991, for Atlantic blocking ridges).

Most past studies of baroclinic instability have assumed that the disturbance has a sinusoidal structure on a zonally uniform current and the amplitude of the wave train grows with time. Without doubt, these studies have illuminated basic physical processes of baroclinic instability. However, since instability occurs over the whole domain for these models, they are not directly applicable to localized phenomena such as the formation of the Kuroshio large meander and atmospheric blocking. From this point of view, localized baroclinic instability problems have been attracting a lot of interest in recent years. One approach is to solve for the linear localized normal modes by assuming that the basic flow is stable except for a limited area wherein the necessary condition for baroclinic instability is locally satisfied (Pedlosky 1989, 1992; Samelson and Pedlosky 1990). Our approach is different. We will consider the evolution of finite amplitude disturbances that are localized initially; even though the basic flow may be stable to infinitesimal disturbances, finite-amplitude solitary waves can be baroclinically unstable *locally* due to their nonlinearity. The effects of nonlinearity are explained in detail later in this section.

Some linear theories have considered the evolution of an initial localized disturbance, with the intent to find out whether instability is absolute or convective

Corresponding author address: Dr. Humio Mitsudera, CSIRO, Division of Atmospheric Research, Private Bag 1, Modialloc, Victoria 3195, Australia.

(e.g., Merkine 1977). The absolute instability means that the disturbance grows and spreads faster than it propagates away from the source, so that at any given point, the disturbance grows with time. On the other hand, in the case of convective instability, the disturbance propagates away more quickly than it spreads, so that the response will vanish from any location after a long enough time. However, in the long-wave limit of weak dispersion, the concept of absolute or convective instability may be useful only while the behavior of localized disturbances is governed by linear dynamics. If the disturbances grow and have finite amplitude, the behavior becomes markedly different as described below from that of linear wave dynamics, particularly due to the dependence of the phase speed on amplitude.

Recently, Kubokawa (1988, 1989) and Mitsudera and Grimshaw (1991a, henceforth referred to as MG) investigated a weakly nonlinear, long-wave theory of baroclinically unstable solitary waves. They used a two-layer model, which consists of a thin upper layer and deep lower layer. They then obtained an evolution equation of the Korteweg-de Vries (KdV) type for the upper-layer motion, with an extra term that represents the coupling with the lower layer, while the lower layer motion is described by a linear long-wave equation (because the motion there is weak), which in turn couples with the upper layer [cf. (2.17) in this paper without friction terms]. It is found that the coupled equations have a steadily propagating solitary wave solution of the form

$$A = a\,\mathrm{sech}^2\left(\frac{a}{2}\right)^{1/2}(x - ct), \qquad (1.1)$$

where a is the amplitude and c is the phase speed of the coupled solitary wave. An important property of finite-amplitude solitary waves is that the phase speed c depends on the amplitude a. In Fig. 1a, we display a typical c in terms of

$$\Gamma = \Delta - 2a, \qquad (1.2)$$

where Δ is the linear long-wave phase speed in the upper layer in the absence of any coupling between the two layers. Note that Γ then represents the phase speed of solitary waves in the upper layer without any coupling (see, e.g., MG). Figure 1a indicates that there are two distinct modes as $\Gamma \to \pm\infty$. One has a phase speed proportional to Γ, so that this represents an upper-layer wave mode. The other has a phase speed independent of Γ, and hence this represents the lower-layer wave mode. However, if the phase speeds of these modes come into close proximity, resonance occurs between the two modes; if the signs of the potential vorticity gradients in the two layers are opposite (i.e. Charney–Stern necessary condition for instability), there is no steady propagation in the range

$$\Gamma_1 < \Gamma < \Gamma_2. \qquad (1.3)$$

In fact, localized baroclinic instability occurs there.

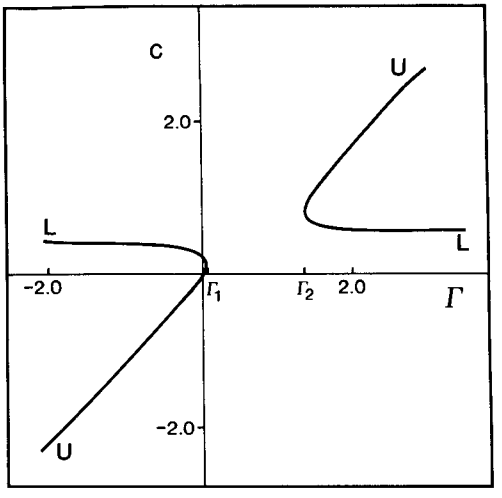

FIG. 1a. Phase speed, c, of a steadily propagating solitary wave in a nonfrictional two-layer model when a basic current has the unstable configuration. The profile of the basic current and parameters is given by (3.13) and (3.14). In this case, $\Gamma_1 = 0.05$ and $\Gamma_2 = 1.35$. The labels "U" and "L" denote upper- and lower-layer branches.

In Fig. 1b we display the behavior of an unstable solitary wave, where $\Gamma_2 = 1.35$ and $\Delta = 1.6$. The initial amplitude is $a = 0.2$ so that (1.3) is satisfied. Note that if $a < 0.12$, then Γ is outside of the range of instability (1.3); this implies that the basic current is unstable only where solitary waves, whose amplitudes are larger than a critical value, exist. The solitary wave grows initially, *with decreasing phase speed as the amplitude increases.* Such dependence of phase speed on amplitude is one of the marked differences from the linear wave. Note that Γ decreases as a increases as well. Thus, the solitary wave in the upper layer is stabilized when it grows sufficiently so that $\Gamma < \Gamma_1$, and propagates neutrally thereafter. But note that as the wave stabilizes, a second solitary wave is generated that also grows and stabilizes because the phase speed of the linear wave in the lower layer is unchanged so that it remains in the unstable range.

The previous studies of Kubokawa and MG assumed that there is no friction. Clearly, friction is an important factor for the nonlinear wave evolution. For a periodic *wave train* case, for example, Pedlosky and Frensen (1980) have shown that in the presence of Ekman friction, a finite-amplitude baroclinic wave exhibits a rich variety of behavior including steady, periodic, and chaotic evolution. In this paper, in contrast to the work of Pedlosky and Frenzen (1980), we will investigate the effects of bottom and interfacial friction on the finite-amplitude *localized* baroclinic waves. In particular, one of our aims is to find whether there are multiple equilibria where conversion of energy due to baroclinic process and frictional dissipation are in balance. Note that the flow is not forced externally, and

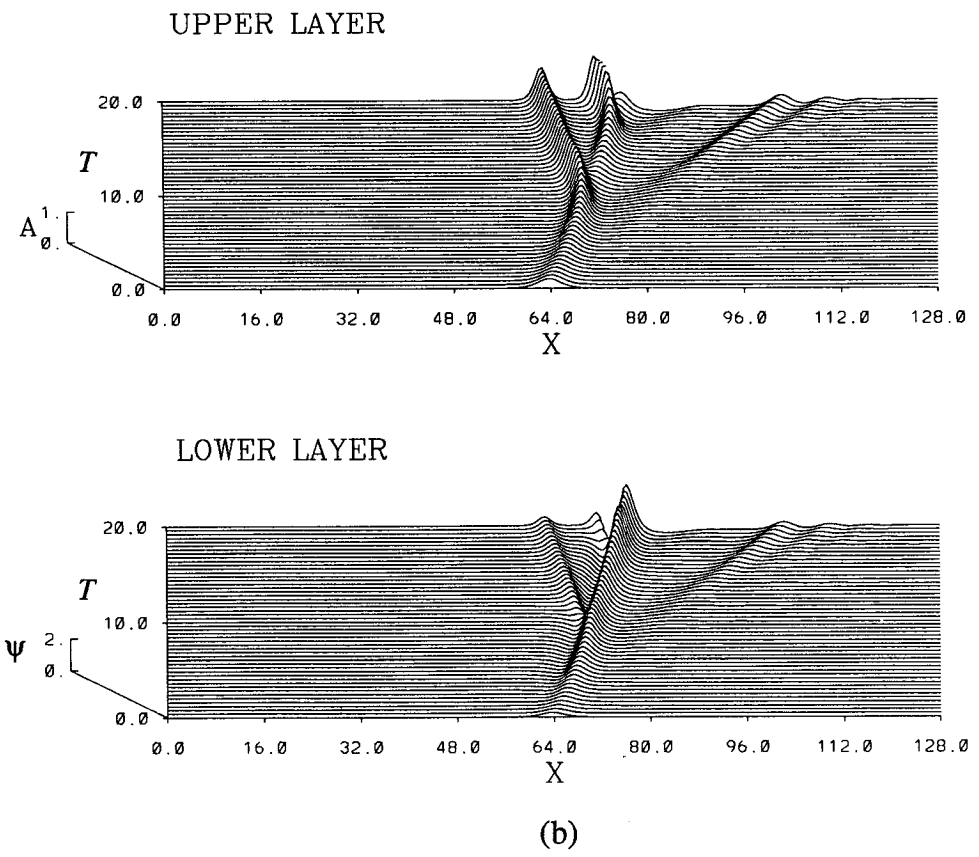

(b)

FIG 1b. The evolution of an unstable solitary wave in the nonfrictional case ($r_1 = r_2 = 0$) obtained by integrating (2.17) directly, where X and T are variables indicating longshore position and time, respectively.

multiplicity here refers to the presence or absence of solitary waves propagating steadily on a zonal flow for a given set of parameters. For this purpose we have derived equations similar to Kubokawa (1989) and MG in section 2, but here we include bottom and interfacial Ekman friction. In nondimensional and scaled form they are given by (2.17a–c).

In section 3 we present a linear stability analysis with bottom and interfacial friction. Although we assume a sinusoidal wave train in section 3, the analysis is found to be useful for the understanding of the nonlinear behavior of localized disturbances. In particular, we have found that if *either* bottom friction alone *or* interfacial friction alone is included, the system may be destabilized in a range where it is neutral otherwise. This somewhat puzzling feature was first found by Holopainen (1961) for a two-layer model (although he considered only bottom friction), and our analysis has shown that this is consistent in the long-wave limit. In the Appendix, we discuss this destabilizing effect of friction from the viewpoint of energetics of the nonlinear equation (2.17). In section 4 we present an analytical solution of the localized instability, assuming that both of the coupling and frictional terms are weak compared with the KdV terms describing temporal evolution, nonlinearity, and dispersion. We thus obtained a perturbed KdV equation for the upper-layer motion, which we have solved approximately using perturbation theory (Karpman and Maslov 1978; Kaup and Newell 1978; Grimshaw and Mitsudera 1992). The main purpose in the section is to find multiple equilibria where baroclinic energy conversion and frictional dissipation are in balance. In section 5, we present various numerical results without restrictions in parameter values, calculated by using a pseudospectral method similar to that developed by Fornberg and Whitham (1978). Results are summarized and some applications are discussed in section 6. A list of symbols is given in Table 1 for convenience.

2. Formulation

We consider a channel filled with a two-layer fluid with average depths $H_{1,2}$ and densities $\rho_{1,2}$ situated on a β plane. Here the subscripts 1 and 2 are associated with the upper and lower layers, respectively. The difference in density between the upper and lower layers is assumed to be small; that is, $\Delta\rho\ (= \rho_2 - \rho_1) \ll \rho_2$.

TABLE 1. List of symbols.

The primes denote nondimensional variables, and the asterisks denote variables either scaling with ϵ or expanded in powers of ϵ. Rescaled variables (without * or ′) are defined in (2.16). Subscripts 1 and 2 denote variables of upper and lower layers, respectively.

A^*, A	Form of waves in the upper layer.
A_s^*, A_s	Solitary wave solution; (2.15a), (4.4a).
$A_{I,B}$	Vertical eddy viscosities of the interface (denoted by I) and bottom (B) (dimensional).
a^*, a	Amplitudes of solitary waves.
$a_\pm$	Amplitudes for steady propagation, where $a_+ > a_-$.
$a_\pm^{(1)}$	Amplitude corrections for steady propagation derived in the perturbation method. In this case, steady amplitudes are expressed as $a_\pm = a^{(0)} + \gamma^{1/2} a_\pm^{(1)}$.
B_n, B	Form of waves in the lower layer.
b	Parameter representing lower-layer potential vorticity gradient; (3.6d).
c^*, c	Phase speeds of waves.
c_U, c_L	Phase speeds of U and L modes.
$c^{(1)}$	Correction to the phase speed in $\gamma^{1/2}$; (4.7).
d_n	Defined in (3.6f).
$E_{I,B}$	Ekman numbers for the interface (I) and bottom (B).
f_0	Typical Coriolis parameter (dimensional).
H_0	Typical depth ($=H_1$) (dimensional).
$H_{1,2}$	Undisturbed upper- and lower-layer thicknesses (dimensional).
I^*	Integral of the upper-layer potential vorticity; (2.13g).
I_B	Baroclinic coupling term for amplitude; (4.5c), (4.10a).
J_B	Baroclinic coupling term for phase speed; (4.5d), (4.10b).
k	Wavenumber for sinusoidal waves.
l^*, l	Half-widths of solitary waves.
L_0	Typical horizontal length scale, taken to the Rossby radius (dimensional).
$-L'$	Position of the offshore boundary.
$p'_{1,2}$	Quasigeostrophic pressure.
$Q'_{1,2}$	Ambient potential vorticities.
$Q_{1,2}^*$, $Q_{1,2}$	Ambient potential vorticities to the lowest order in ϵ.
q_n	Phase speed of the nth mode of the lower-layer wave if there is not any coupling.
Ro	Rossby number.
r	Coefficient for friction when $r_1 = \gamma r_2$.
r_1^*, r_1	Coefficients for interfacial friction; (2.13f), (2.16).
r_2	Coefficient for bottom friction; (2.16).
S	Time-dependent phase difference between the upper- and lower-layer motions multiplied by l.
T^*	Time scaling with ϵ^3; (2.6).
T_B	Time scale of baroclinic growth (dimensional).
T_s	Time scale of the evolution of solitary waves (dimensional).
U_0	Typical speed of the upper-layer mean current (dimensional).
U'_1	Upper-layer mean current.
U_1^*, U_1	Upper-layer mean current of the leading order in ϵ, whose speeds at the coastal and offshore boundaries are zero; (2.9).
$U_1^{(1)*}$, $U_1^{(1)}$	Corrections to the upper-layer mean current; (2.9).
U'_2, U_2^*, U_2	Lower-layer mean current.
x', X^*, X	Longshore coordinates.
y'	Cross-channel coordinates.
Δ^*, Δ	Linear long-wave phase speed of the upper layer; (2.13b), (2.16).
Γ	Phase speed of the solitary wave in the upper layer if there is no coupling between the two layers; (1.2).
$\Gamma_{1,2}$	Margins of instability in Γ; $\Gamma_1 < \Gamma_2$.
Ω	Function of α defined by (4.14b). Baroclinic conversion is given by $I_B = -a^2 b \Omega(\alpha)/2r_2$ when steady.
Φ	Function of S defined by (4.27d), which is related to J_B.
Π	Function of S defined by (4.27c), which is related to I_B.
α	$c^{(1)} l / r_2$ as defined by (4.14c).
$\pm\alpha_e$	Values of α for steady propagation.
β', β^*, β	Parameter for the planetary beta effect.
χ	Function of α defined by (4.17b).
δ_E	Ekman layer thickness (dimensional).
δa, $\delta c^{(1)}$, δS, etc.	Perturbation from their equilibrium.
ϵ	Parameter characterizing long waves ($\ll 1$).
η_n	Cross-channel structure of the lower-layer waves.
γ', γ^*, γ	Ratio of the thicknesses of the upper and lower layers.
κ^*	Coupling coefficient between the two layers; (2.13e).
λ	$c_U - c_L$ in (3.8d).
$\pm\lambda_0$	Branch points on the λ-Rieman surface; (3.8e).
λ_d^*	Dispersive coefficient; (2.13d).
μ^*	Nonlinear coefficient; (2.13c).

TABLE 1. (*Continued*)

The primes denote nondimensional variables, and the asterisks denote variables either scaling with ϵ or expanded in powers of ϵ. Rescaled variables (without * or ') are defined in (2.16). Subscripts 1 and 2 denote variables of upper and lower layers, respectively.

ν, ν_N	Factors of the interfacial friction influencing the lower-layer motion.
ν_I^*, ν_I	Scaled Ekman numbers of the interface.
ν_B^*, ν_B	Scaled Ekman numbers of the bottom.
ϕ^*	Cross-channel structure of the upper-layer waves.
ψ_1'	Streamfunction of the upper layer.
ψ_2'	Streamfunction of the lower layer.
ψ^*, ψ	Streamfunction of the lower layer to the leading order in ϵ.
ρ	Parameter related to frictional dissipation; $\rho = \Omega(\alpha)$ determines steady solutions; (4.20a).
σ	Ratio of upper- and lower-layer densities.
τ	Time scaling with $\gamma^{1/2}$; (4.1).
θ	Phase of the solitary wave.

We shall use a nondimensional coordinate system given in Fig. 2, based on a length scale L_0; a depth scale H_0 ($= H_1$), which is typical for the upper layer; a time scale L_0/U_0, where U_0 is a typical mean current speed in the upper layer; and a typical Coriolis parameter f_0. For the horizontal length scale L_0 we use the internal Rossby radius of deformation $[(\Delta\rho/\rho_2)gH_0]^{1/2}/|f_0|$, where g is the acceleration due to gravity.

We suppose that $p_{1,2}'$ is the nondimensional geostrophic pressure scaled by $\rho_{1,2}f_0L_0U_0$. Here, the prime denotes nondimensional variables. We then separate the mean current from the perturbed field such that

$$p_{1,2}' = \int_{y'}^{0} U_{1,2}'(\hat{y})d\hat{y} + \psi_{1,2}'. \tag{2.1}$$

Thus the perturbations $\psi_{1,2}'$ satisfy

$$\left(\frac{\partial}{\partial t'} + U_1'\frac{\partial}{\partial x'}\right)[\nabla^2\psi_1' - (\psi_1' - \psi_2')] + J(\psi_1', \nabla^2\psi_1' - (\psi_1' - \psi_2')) + Q_{1y'}'\psi_{1x'}' = -\frac{E_I^{1/2}}{\mathrm{Ro}}\nabla^2(\psi_1' - \psi_2'), \tag{2.2a}$$

$$\left(\frac{\partial}{\partial t'} + U_2'\frac{\partial}{\partial x'}\right)[\nabla^2\psi_2' - \gamma'(\psi_2' - \sigma\psi_1')] + J(\psi_2', \nabla^{2\prime}\psi_2' - \gamma'(\psi_2' - \sigma\psi_1')) + Q_{2y'}'\psi_{2x'}'$$

$$= -\frac{\gamma' E_B^{1/2}}{\mathrm{Ro}}\nabla^2\psi_2' + \frac{\gamma' E_I^{1/2}}{\mathrm{Ro}}\nabla^2(\psi_1' - \psi_2'), \tag{2.2b}$$

where

$$Q_{1y'}' = \beta' - U_{1y'y'}' + U_1' - U_2', \tag{2.2c}$$

$$Q_{2y'}' = \beta' - U_{2y'y'}' + \gamma'(U_2' - \sigma U_1'), \tag{2.2d}$$

$$J(a, b) = a_{x'}b_{y'} - a_{y'}b_{x'}. \tag{2.2e}$$

Here, $\sigma = \rho_1/\rho_2$ and β' is the meridional gradient of the Coriolis parameter scaled by $U_0L_0^{-2}$, and γ' is the depth ratio between the two layers,

$$\gamma' = \frac{H_1}{H_2}. \tag{2.3a}$$

Note that from (2.2b), we see that γ' measures the strength of the coupling between the upper and the lower layers. The Rossby number, Ro, is

$$\mathrm{Ro} = \frac{U_0L_0}{f_0}, \tag{2.3b}$$

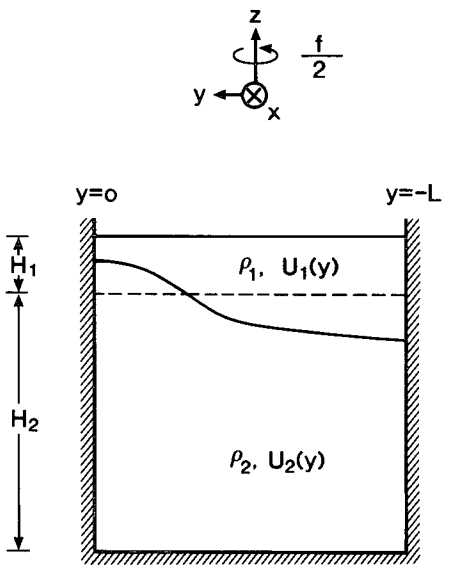

FIG. 2. Nomenclature and coordinate system.

while $E_{I,B}$ are the interfacial and bottom Ekman numbers such that

$$E_{I,B} = \frac{A_{I,B}}{2f_0 H_0^2 \rho_{1,2}}, \tag{2.3c}$$

where A_I and A_B are vertical eddy viscosities at the interface and bottom, respectively. The terms in (2.2a,b) multiplied by $E_I^{1/2}/Ro$ represent interfacial friction, which tends to reduce the vorticity difference between the two layers, or it tends to damp internal (baroclinic) motion. Bottom friction is represented by the term multiplied by $E_B^{1/2}/Ro$ in (2.2b), which reduces vorticity of the barotropic motion. We suppose that the channel boundaries are placed at $y' = 0$ and $-L'$. Thus the boundary conditions become

$$\psi'_{1,2} = 0; \quad \text{at} \quad y' = 0, -L'. \tag{2.4}$$

If the offshore boundary at $y' = -L'$ is removed, the boundary conditions are changed to $\psi'_{1,2} < \infty$ as $y' \to -\infty$. If $\beta' = 0$ (or more accurately, $Q'_{1,2y'} \to 0$ as $y' \to 0$), then $\psi' \to 0$ as $y' \to -\infty$, and hence the boundary conditions are basically unchanged. If $\beta' \neq 0$, however, radiation of energy due to Rossby waves may occur. This could also cause significant damping effects; some discussion is given in section 6. Retaining the offshore boundary removes this radiational damping, and hence we will focus on the effects of friction alone.

In this paper we study the weakly nonlinear evolution of long waves. Thus, we rescale the longshore variable x' and introduce a new variable such that

$$X^* = \varepsilon x', \tag{2.5}$$

where ε is a small parameter. Here, the asterisk denotes variables either scaling with ε, or expanded in powers of ε. In physical terms, ε^{-1} measures the wavelength with respect to the internal Rossby radius of deformation. Further, for simplicity, we will suppose that γ' is small, which implies that the lower layer is much deeper than the upper layer. Thus, we put $\gamma' = \varepsilon^2\gamma^*$. This means from (2.2b) that the coupling between the two layers is weak. Furthermore, we retain $Q'_{2y'}$ (2.2d) to be the same order as the coupling term, and therefore we replace β' and U'_2 with $\varepsilon^2\beta^*$ and $\varepsilon^2 U_2^*$, respectively. Oceanic relevance of this scaling is discussed in section 6. In this situation, the lower-layer wave has a phase velocity of $O(\varepsilon^2)$; therefore, baroclinic instability occurs if the upper-layer wave has a phase speed of $O(\varepsilon^2)$ (e.g., see MG). Thus, we define a slow time scale such that

$$T^* = \varepsilon^3 t'. \tag{2.6}$$

Further, we assume that the time scale due to interfacial and bottom friction is measured by (2.6), so that we replace $E_I^{1/2}/Ro$ and $E_B^{1/2}/Ro$ with $\varepsilon^3\nu_I^*$ and $\varepsilon\nu_B^*$, respectively.

Suppose that there is a mode in the upper layer whose phase speed c' is $O(\varepsilon^2)$. Then, we may expand $\psi'_{1,2}$ as follows:

$$\psi'_1 = \varepsilon^2 A^*(X^*, T^*)\phi^*(y') + \varepsilon^4\psi_1^{(1)^*} + \cdots, \tag{2.7a}$$

$$\psi'_2 = \varepsilon^4\psi_2^* + \cdots, \tag{2.7b}$$

where ϕ^* represents cross-channel structure, which satisfy the following eigenvalue problem where the eigenvalue is zero:

$$U'_1\phi^*_{y'y'} - U'_{1y'y'}\phi^* = 0, \tag{2.8a}$$

$$\phi^* = 0, \quad \text{at} \quad y' = 0, -L'. \tag{2.8b}$$

Equations (2.8a,b) show that if $U'_1(0) = U'_1(-L') = 0$, ϕ^* may be proportional to U'_1. Thus we may suppose here that $U'_1(0)$, $U'_1(-L')$ are $O(\varepsilon^2)$, so that we rewrite $U'_1(y')$ as

$$U'_1 = U_1^*(y') + \varepsilon^2 U_1^{(1)^*}(y'), \tag{2.9}$$

where $U_1^*|_{y'=0,-L'} = 0$, and $U_1^{(1)^*}|_{y'=0,-L'} \neq 0$. Hence we obtain

$$\phi^* = U_1^*(y'), \tag{2.10a}$$

$$Q^*_{1y'} = U_1^* - U^*_{1y'y'}. \tag{2.10b}$$

Substituting (2.7a,b) into (2.2a), we find for the upper-layer motion that

$$U_1^*(\psi^*_{1y'y'X^*} - \psi^*_{1X^*}) + Q^*_{1y'}\psi^*_{1X^*} + M^* = 0, \tag{2.11a}$$

where

$$\begin{aligned} M^* = {} & (\phi^*_{y'y'} - \phi^*)A^*_{T^*} + [(\phi U^{(1)^*}_{1y'y'} - \phi^*_{y'y'}U_1^{(1)^*}) \\ & + (\beta^* - U_2^*)\phi^*]A^*_{X^*} \\ & + (\phi^*_{y'y'y'y'}\phi^* - \phi^*_{y'}\phi^*_{y'y'})A^*A^*_{X^*} \\ & + U_1^*\phi^*A^*_{X^*X^*X^*} \\ & + \phi^*\psi^*_{2X^*} + \nu_I^*A^*\phi^*_{y'y'}. \end{aligned} \tag{2.11b}$$

The boundary conditions for $\psi_1^{(1)^*}$ are

$$\psi_1^{(1)^*} = 0, \quad \text{at} \quad y' = 0, -L'. \tag{2.11c}$$

Thus, (2.11a–c) can be solved when

$$\int_{-L'}^{0} M^* dy' = 0. \tag{2.12}$$

Considering (2.10a), (2.11b), and (2.12), we obtain an evolution equation for the upper-layer motion as follows:

$$\begin{aligned} -(A^*_{T^*} + \Delta^*A^*_{X^*}) + \mu^*A^*A^*_{X^*} + \lambda_d^*A^*_{X^*X^*X^*} \\ + \kappa^*\int_{-L'}^{0} U_1^*\psi^*_{2X^*}dy' - r_1^*A^* = 0, \end{aligned} \tag{2.13a}$$

where

$$I^*\Delta^* = -[U_1^{(1)*} U_{1y'}^*]_{-L'}^0 - \int_{-L'}^0 (\beta^* - U_2^*) U_1^* dy', \tag{2.13b}$$

$$I^*\mu^* = -[U_{1y}^{*2}]_{-L'}^0, \tag{2.13c}$$

$$I^*\lambda_d^* = \int_{-L'}^0 U_1^{*2} dy', \tag{2.13d}$$

$$I^*\kappa^* = 1, \tag{2.13e}$$

$$I^* r_1^* = -\nu_I^* [U_{1y}^*]_{-L'}^0, \tag{2.13f}$$

where

$$I^* = [Q_1^*]_{-L'}^0 = \int_{-L'}^0 U_1^* dy' - [U_1^*]_{-L'}^0. \tag{2.13g}$$

For the lower-layer motion, substituting (2.7a,b) and (2.10a) into (2.2b) yields

$$\left(\frac{\partial}{\partial T^*} + U_2^* \frac{\partial}{\partial X^*}\right)(\psi_{2y'y'}^* + \sigma\gamma^* A^* U_1^*) + Q_{2y}^* \psi_{2X^*}^* + \gamma^* \nu_B^* \psi_{2y'y'}^* - \gamma^* \sigma \nu_I^* A^* U_{1y'y'}^* = 0, \tag{2.14a}$$

$$\psi_2^* = 0 \quad \text{at} \quad y' = 0, -L'. \tag{2.14b}$$

Thus, we have obtained an evolution equation of the KdV type for the upper-layer motion and a linear equation for the lower-layer motion. This is a consequence of the assumption that the lower layer is much deeper than the upper layer, so that the lower-layer motion is much weaker than the upper-layer motion. Similar coupled equations without the frictional terms have been derived by Kubokawa (1988, 1989) and MG, and some features of the solutions were described in the Introduction. On the other hand, (2.13a) without the coupling term has been extensively studied by using perturbation methods, either based on the inverse scattering transform (e.g., Karpman and Maslov 1978; Kaup and Newell 1978) or with multiscale methods (e.g., Grimshaw 1979; Kodama and Albowitz 1981; Grimshaw and Mitsudera 1992). It has been found that a solitary wave amplitude varies in a manner consistent with energetic considerations but that the solitary wave cannot conserve mass by itself, and a shelf forms behind the solitary wave to satisfy mass conservation. In this paper, however, we will not go into details on this aspect and instead will concentrate on the behavior of a solitary wave itself, that is, the evolution of its amplitude and phase speed.

Here, we shall assume that I^* in (2.13g) is positive. This is the case for a jetlike current flowing in the positive direction ($U_1^* > 0$ for $-L' < y' < 0$) because in (2.13g), $U_{1y'}^*(0) < 0$ and $U_{1y'}^*(-L') > 0$. The parameter Δ^* (2.13b) represents a linear, long-wave phase speed in the absence of any coupling between the two layers, nonlinearity and dispersion. From (2.13b), Δ^* is caused by the $O(\varepsilon^2)$ velocity $U_1^{(1)*}$ at the coast, the bottom mean current U_2^*, and the β^* effect. For example, if β^* and U_2^* are set to zero, Δ^* is positive if $U_1^{(1)*}$ is positive for a jetlike current. Note that baroclinic instability occurs in a certain range of Δ^*. The parameter λ_d^* (2.13d) is the dispersive coefficient, which is always positive as I^* is positive. The coefficient r_1^* (2.13f) represents the interfacial friction, which is positive since $[U_{1y}^*]_{-L'}^0 < 0$. The parameter μ^* (2.13c) is the nonlinear coefficient. Note that $\mu^* = 0$ if the basic flow U_1^* is symmetric. In the present study, we assume an asymmetric basic flow so that μ^* is not zero. In this case μ^* is negative (positive) if the shear at $y' = 0$ ($y' = -L'$) is stronger. The sign of μ^* is important because it determines the polarity of solitary waves. In fact, the KdV equation (2.13a) without the coupling and frictional terms has a solution of the form

$$A_s^* = a^* \operatorname{sech}^2 l^*(X^* - c^* T^*), \tag{2.15a}$$

where

$$\Delta^* - c^* = \mu^* a^*/3 = 4\lambda_d^* l^{*2}. \tag{2.15b}$$

Here a^* is the amplitude and c^* is the speed. From (2.15b) and noting that $\lambda_d^* > 0$, $a^*\mu^* > 0$ is necessary to form the solitary disturbance in the form (2.15a). Therefore, the polarity of the solitary disturbance is positive (negative) if μ^* is positive (negative). This suggests that only a cyclonic eddy would form in an eastward oceanic current with a northern boundary, such as Kuroshio, because $\mu^* < 0$ (i.e., $U_{1y'}^* \sim 0$ as $y' \to -\infty$).

Before proceeding further, we shall rescale (2.13) and (2.14) for convenience. We put

$$T = \lambda_d^* T^*, \quad X = X^*, \quad A = \frac{\mu^*}{6\lambda_d^*} A^*,$$

$$\psi = \frac{\mu^*}{6\lambda_d^{*2}} \psi_2^*, \quad \Delta = \frac{\Delta^*}{\lambda_d^*}, \quad U_1 = \kappa^* U_1^*, \tag{2.16}$$

$$U_1^{(1)} = \frac{U_1^{(1)*}}{\lambda_d^*}, \quad U_2 = \frac{U_2^*}{\lambda_d^*}, \quad \beta = \frac{\beta^*}{\lambda_d^*},$$

$$\gamma = \frac{\gamma^*\sigma}{\kappa^*\lambda_d^*}, \quad r_1 = \frac{r_1^*}{\lambda_d^*}, \quad \nu_I = \frac{\nu_I^*}{\lambda_d^*}, \quad r_2 = \kappa^* \frac{\nu_B^*}{\sigma}.$$

The rescaled equations are thus

$$-(A_T + \Delta A_X) + 6AA_X + A_{XXX} + \int_{-L}^0 U_1 \psi_X dy - r_1 A = 0, \tag{2.17a}$$

$$\left(\frac{\partial}{\partial T} + U_2 \frac{\partial}{\partial X}\right)(\psi_{yy} + \gamma A U_1) + Q_{2y}\psi_X + \gamma r_2 \psi_{yy} - \gamma \nu r_1 A U_{1yy} = 0, \tag{2.17b}$$

$$\psi(0) = \psi(-L) = 0, \tag{2.17c}$$

where

$$Q_{2y} = \beta - U_{2yy} - \gamma U, \tag{2.17d}$$

$$\nu = -1/[U_{1y}^{(0)}]_{-L}^{0}. \tag{2.17e}$$

Here, and in what follows, we drop the primes from y' and L' for neatness. Note that ν is positive.

3. Linear stability in the presence of friction

Before considering the nonlinear problem and the multiple equilibria of (2.17), we will discuss the stability properties of the linearized version of (2.17). There are two important relations between the linear and nonlinear analyses. First, as mentioned in the Introduction, bottom and interfacial friction can destabilize rather than damp the otherwise neutral waves. Holopainen (1961) found this phenomenon by considering bottom friction alone. Here, we include both bottom and interfacial friction, and will show that this conclusion is also consistent in the long-wave limit, if the magnitudes of bottom and interfacial friction are considerably different. As shown later in sections 4 and 5, this effect is also seen in the nonlinear evolution of solitary waves. Second, the marginal values of the nonlinear instability band, $\Gamma_{1,2}$ in (1.3) (see also Fig. 1a), approximate to those obtained by the linear stability analysis if both bottom and interfacial friction are small. Hence, from linear analyses we may evaluate amplitudes of solitary waves at marginal stability, using the formulas $\Gamma_{1,2} = \Delta - 2a$ (1.2) for a given Δ.

Now, to solve (2.17) we expand ψ such that

$$\psi = \sum_{n=1}^{\infty} B_n(X, T)(U_2 - q_n)\eta_n(y), \tag{3.1}$$

where $\eta_n(y)$ satisfies the following eigenvalue problem where q_n is the eigenvalue:

$$[(U_2 - q_n)\nu_n]_{yy} + Q_{2y}\eta_n = 0, \tag{3.2a}$$

$$\eta_n = 0 \quad \text{at} \quad y = 0, -L. \tag{3.2b}$$

The orthogonality condition is

$$\int_{-L}^{0} Q_{2y}\eta_n\eta_m dy = 0 \quad \text{for} \quad n \neq m, \tag{3.3a}$$

and η_n is normalized by

$$\int_{-L}^{0} \eta_{ny}^2 dy = 1. \tag{3.3b}$$

Substituting (3.1) into (2.17a) without the nonlinear and dispersive terms for the upper-layer motion, and into (2.17b), and applying the orthogonality condition (3.3a) for the lower-layer motion, yields

$$-(A_T + \Delta A_X) - r_1 A + \sum_{n=1}^{\infty} B_{nX} \times \int_{-L}^{0} (U_2 - q_n)\eta_n U_1 dy = 0, \tag{3.4a}$$

$$-(B_{nT} + q_n B_{nX} + \gamma r_2 B_n)\int_{-L}^{0} Q_{2y}\eta_n^2 dy + \gamma \int_{-L}^{0} (A_T + U_2 A_X)U_1\eta_n dy - \gamma\nu r_1 A \int_{-L}^{0} U_{1yy}\eta_n dy = 0, \tag{3.4b}$$

respectively. First, we would like to discuss the qualitative features of (3.4). Especially, we wish to retain γ and $r_{1,2}$ as O(1) parameters. For this reason we assume that only a single mode ($n = N$, say) in the lower layer couples strongly with an upper-layer wave; normally, the lowest mode (i.e., $N = 1$) couples most strongly. Thus we put

$$\psi \approx B_N(U_2 - q_N)\eta_N. \tag{3.5}$$

Further, we assume that U_2 is a constant for simplicity. Later in this section, we will present numerical calculations of the eigenvalue problem (2.17) where the nonlinear and dispersive terms are omitted. The results show that the truncation (3.5) is relevant with $N = 1$ for a jetlike upper-layer mean flow. Thus, we consider the following equation here:

$$-(A_T + \Delta A_X) - r_1 A + B_X = 0, \tag{3.6a}$$

$$-(B_T + q_N B_X + \gamma r_2 B) + \frac{\gamma b}{U_2 - q_N} \times (A_T + U_2 A_X + \nu' r_1 A) = 0, \tag{3.6b}$$

where

$$B = d_N B_N, \tag{3.6c}$$

$$b = d_N^2 \Big/ \int_{-L}^{0} Q_{2y}\eta_N^2 dy = -d_N^2(q_N - U_2)^{-1}, \tag{3.6d}$$

$$\nu_N = -\nu \int_{-L}^{0} U_{1yy}\eta_N dy \Big/ \int_{-L}^{0} U_1\eta_N dy, \tag{3.6e}$$

and

$$d_N = \int_{-L}^{0} (U_2 - q_N)U_1\eta_N dy. \tag{3.6f}$$

Note that ν_N, like ν, is positive.

Now, let us find a solution of the form

$$\begin{pmatrix} A \\ B \end{pmatrix} = \begin{pmatrix} A_0 \\ B_0 \end{pmatrix} e^{ik(X-cT)}. \tag{3.7}$$

Although we are using a sinusoidal disturbance here, we will find that the analysis is very useful for interpreting the behavior of a solitary disturbance. Substituting (3.7) into (3.6a,b) we may obtain the speed c as follows:

$$c = \frac{1}{2}(c_U + c_L) \pm \frac{1}{2}(\lambda^2 - \lambda_0^2)^{1/2}, \quad (3.8a)$$

where

$$c_U = \Delta + \frac{\gamma b}{q_N - U_2} - \frac{ir_1}{k}, \quad (3.8b)$$

$$c_L = q_N - \frac{i\gamma r_2}{k}, \quad (3.8c)$$

$$\lambda = c_U - c_L, \quad (3.8d)$$

$$\lambda_0^2 = -4b\gamma\left[1 + \frac{i}{k(q_N - U_2)}(\nu_N r_1 - \gamma r_2)\right]. \quad (3.8e)$$

We consider here the behavior of c as Δ varies. As $|\Delta| \to \infty$ (i.e., $\lambda \to \infty$), c represents two distinct modes—c_U and c_L. In this situation the motion is concentrated on the upper (lower) layer for the wave represented by c_U (c_L). We shall call the wave with c_U the U mode, and the wave with c_L the L mode. As $|\mathrm{Re}(\lambda)| \to 0$, that is, when the phase speed of the U mode and L mode are almost coincident, the behavior of c, with varying Δ, depends on the sign of b. In fact, if $r_1 = r_2 = 0$, we can see from (3.8) that the system is stable for all Δ for positive b, while there is instability for $|\lambda| < 2(-b\gamma)^{1/2}$ for negative b. Note here that for negative b, Q_{2y} must be negative somewhere [see (3.6d)], which is the well-known necessary condition for baroclinic instability.

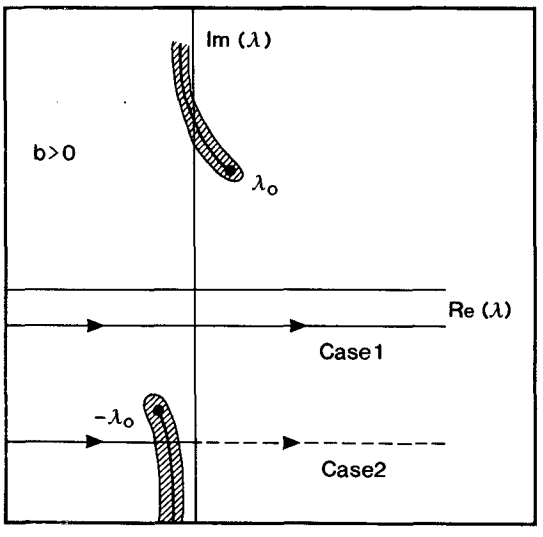

FIG. 3. Loci of λ on the upper Riemann surface as Δ varies when the basic current has a stable configuration [i.e., $b > 0$, where b is defined in (3.6d)]. Shaded lines are branch cuts where $\sqrt{\lambda^2 - \lambda_0^2}$ is real. The dashed line indicates that the locus of λ in case 2 passes onto the lower Riemann surface as Δ varies.

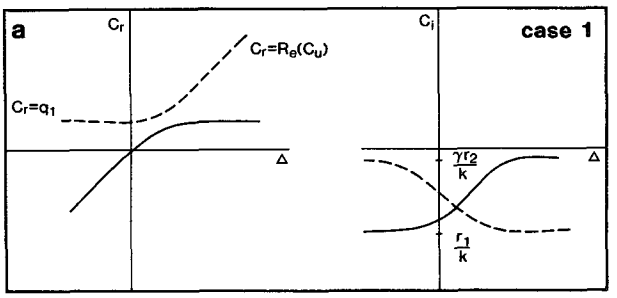

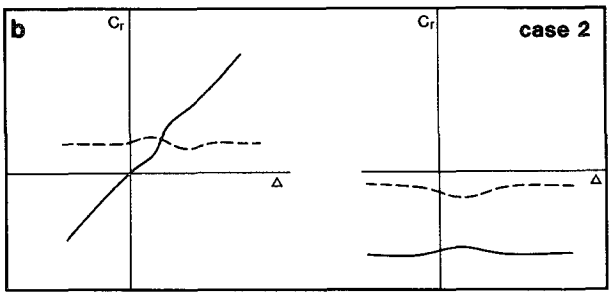

FIG. 4. Schematic plots of c as Δ varies when $b > 0$ and $U_2 > 0$; c_r and c_i represent $\mathrm{Re}(c)$ and $\mathrm{Im}(c)$: (a) case 1 and (b) case 2.

Let us examine the cases for positive b first. From (3.8a) we obtain two branch points on the λ-Riemann surface—$\lambda = \pm\lambda_0$. Further, we insert branch cuts where $\mathrm{Re}(\sqrt{\lambda^2 - \lambda_0^2}) = 0$, and define the upper Riemann surface by $\mathrm{Re}(\sqrt{\lambda^2 - \lambda_0^2}) > 0$. As shown in Fig. 3 there are typically two cases in the behavior of λ as Δ varies, depending on the relative magnitude between $\mathrm{Im}(\lambda)$ and $\mathrm{Im}(\lambda_0)$. Without loss of generality we can assume that $\mathrm{Im}(\lambda) < 0$ (i.e., $\gamma r_2 < r_1$) as well as $\mathrm{Im}(\lambda_0) < 0$ [i.e., $\gamma r_2 < \nu_N r_1$, where we note that $b > 0$ implies that $q_N < U_2$ from (3.6d)]; we see that this assumption corresponds to the situation of Fig. 3. Suppose $\mathrm{Re}(\sqrt{\lambda^2 - \lambda_0^2}) > 0$ as $\Delta \to -\infty$. In case 1 where $|\mathrm{Im}(\lambda)| < |\mathrm{Im}(\lambda_0)|$, λ remains on the upper Riemann surface as $\Delta \to \infty$, and therefore, $\mathrm{Re}(\sqrt{\lambda^2 - \lambda_0^2})$ is always positive. In case 2, however, λ passes onto the lower Riemann surface, so that $\mathrm{Re}(\sqrt{\lambda^2 - \lambda_0^2})$ becomes negative as $\Delta \to \infty$. Noting that $\mathrm{Re}(\lambda)$ is negative (positive) as $\Delta \to -\infty$ (∞), we obtain

$$\sqrt{\lambda^2 - \lambda_0^2} \sim \begin{cases} -\lambda, & \text{as } \Delta \to -\infty \\ \begin{cases} \lambda \text{ (case 1)} \\ -\lambda \text{ (case 2)}, \end{cases} & \text{as } \Delta \to \infty. \end{cases} \quad (3.9)$$

Therefore, c asymptotically becomes

$$c \sim \begin{cases} (c_L, c_U), & \text{as } \Delta \to -\infty \\ \begin{cases} (c_U, c_L) \text{ (case 1)} \\ (c_L, c_U) \text{ (case 2)}, \end{cases} & \text{as } \Delta \to \infty, \end{cases} \tag{3.10}$$

and hence, for case 1, the exchange of modes occurs in the vicinity of $\mathrm{Re}(\lambda) = 0$, while the exchange does not occur for case 2. Recall that $\mathrm{Re}(\lambda) = 0$ occurs when the real phase speed of U and L modes are coincident, that is, when $q_N = \Delta + \gamma b(q_N - U_2)^{-1}$. To seek the behavior of c near $\mathrm{Re}(\lambda) = 0$, we assume $|\nu_N r_1 - \gamma r_2| \ll 1$ in λ_0^2 (3.8e) for simplicity. Then the growth rate at $\mathrm{Re}(\lambda) = 0$ becomes

$$\mathrm{Im}(c) = -\frac{1}{2k}(r_1 + \gamma r_2) \quad \text{(case 1)} \tag{3.11a}$$

$$= -\frac{1}{2k}[(r_1 + \gamma r_2) \pm \sqrt{(r_1 - \gamma r_2)^2 - 4k^2\gamma b}] \quad \text{(case 2)}. \tag{3.11b}$$

Thus, $\mathrm{Im}(c)$ is always negative if $b > 0$. In Fig. 4 we display schematic plots for the two cases for $U_2 > 0$. Features expressed in Fig. 4 are common for linearly coupled damped oscillators (Grimshaw and Allen 1982) and have been found for coastally trapped waves (Mitsudera and Hanawa 1989).

If $b < 0$, there is instability for the nonfrictional case as mentioned before. To consider the frictional cases we display the loci of λ as Δ varies in Fig. 5 for negative b. There are also two cases as $\Delta \to \infty$, depending on the relative magnitudes of $\mathrm{Im}(\lambda)$ and $\mathrm{Im}(\lambda_0)$. In the vicinity of $\mathrm{Re}(\lambda) = 0$, the growth rate is written as (3.11b) for both cases if $b < 0$, and there is instability if the second term on the right-hand side of (3.11b) is larger than the first term or when $-k^2 b > \gamma r_1 r_2$. In particular, if the frictional coefficients are small, there is always instability near $\mathrm{Re}(\lambda) = 0$ since

$$\mathrm{Im}(c) \approx \pm\sqrt{-\gamma b}, \quad \text{at} \quad \mathrm{Re}(\lambda) = 0. \tag{3.12}$$

Recall that c behaves as in (3.10) asymptotically as $|\Delta| \to \infty$. Thus we may describe the schematic behavior of c in terms of Δ for $U_2 = 0$ as in Fig. 6. Note that if either $r_1 \to 0$ and $r_2 \neq 0$ or $r_2 \to 0$ and $r_1 \neq 0$, then either $\mathrm{Im}(c_L)$ or $\mathrm{Im}(c_U)$ is zero, so that one of $\mathrm{Im}(c)$ in (3.8a) approaches zero smoothly as $|\Delta| \to \infty$. Therefore, the range of instability in terms of Δ may become infinite. Recall here that when $r_1 = r_2 = 0$, the instability range is restricted to $|\mathrm{Re}(\lambda(\Delta))| < 2(-b\gamma)^{1/2}$ from (3.8b). Therefore, if either only bottom friction or only interfacial friction is included, the system is destabilized in a range where it is stable otherwise. This result agrees with that obtained by Holopainen (1961), who found a widening of the instability range in wavenumber when bottom friction is included.

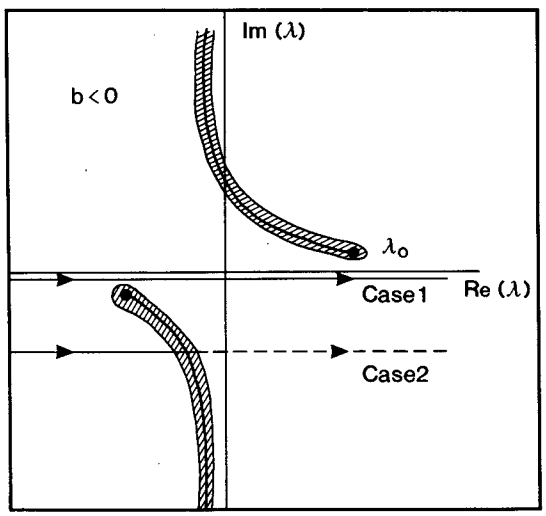

FIG. 5. Loci of λ on the upper Riemann surface as Δ varies when the basic current has an unstable configuration (i.e., $b < 0$).

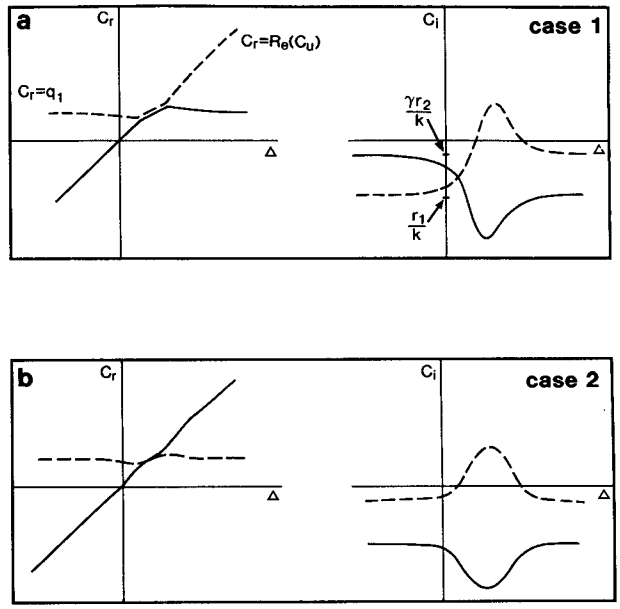

FIG. 6. Schematic plots of c as Δ varies when $b < 0$ and $U_2 = 0$: (a) case 1 and (b) case 2.

In Fig. 7, we display instability diagrams for typical cases of negative b. To calculate these eigenvalues, we used a channel with $L = 2$, or in the dimensional term, the channel is twice as wide as the Rossby radius of deformation. The current profile was given by

$$U_1 = -\left(\pi + \frac{4}{\pi}\right)^{-1}\left(\sin\frac{\pi}{2}y + \frac{1}{8}\sin\pi y\right), \quad \text{for} \quad -2 < y < 0. \tag{3.13}$$

Note that from the definition (2.16), the amplitude of the basic current is fixed. This is an asymmetric jet

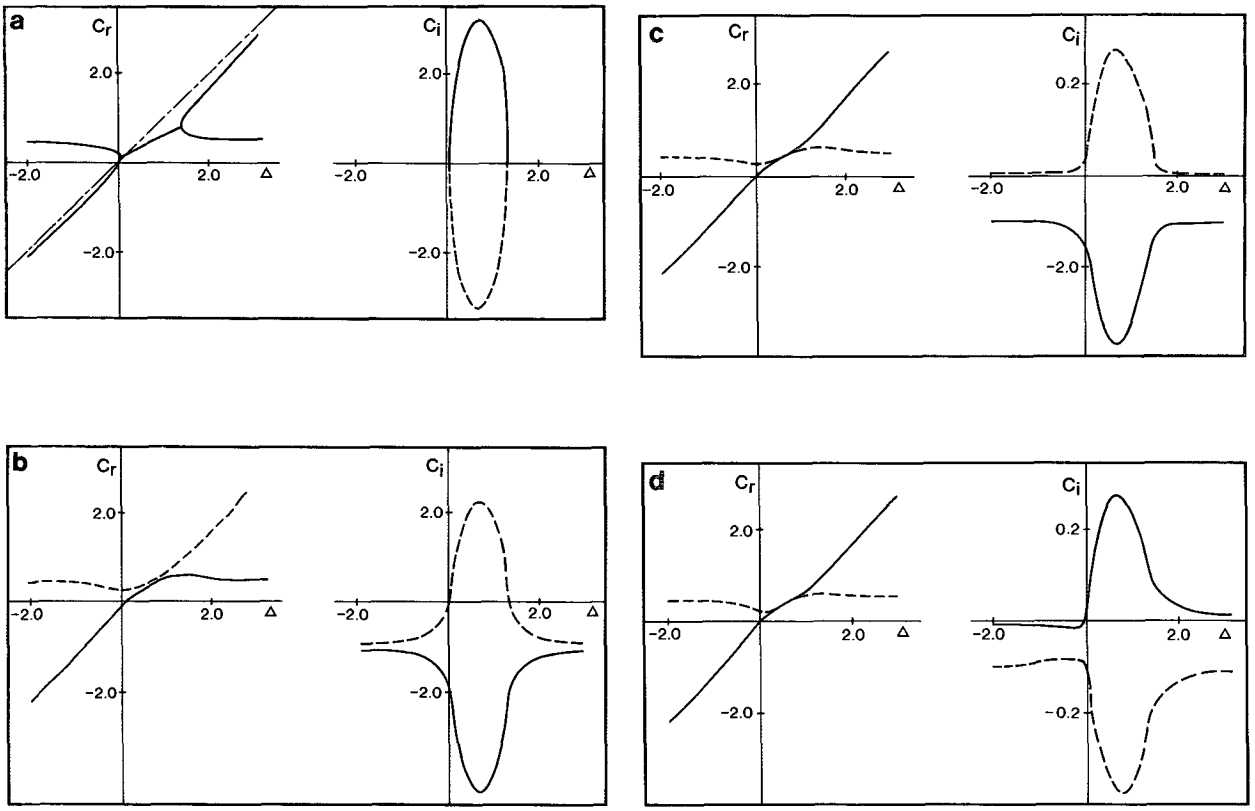

FIG. 7. Numerical examples of c, for typical cases when $b < 0$. Parameter values are (3.13) and (3.14); (a) $r_1 = \gamma r_2 = 0$. Dashed-dotted line indicates $c = \Delta$, which is drawn for comparison purposes only; (b) $r_1/k = \gamma r_2/k = 0.1$. (c) $r_1/k = 0.1$, $\gamma r_2/k = 0$. (d) $r_1/k = 0$, $\gamma r_2/k = 0.1$.

with the velocity maximum at $y = -0.79$. Recall that the upper-layer wave has a phase speed equal to zero to the lowest order in ε for the velocity profile (3.13) because $U_1(0) = U_1(-L) = 0$ [see (2.10a)]. For the depth ratio parameter, we used

$$\gamma = \gamma_0\left(\pi + \frac{4}{\pi}\right), \tag{3.14a}$$

where

$$\gamma_0 = 2.5, \tag{3.14b}$$

and

$$\beta = 1.0, \quad U_2 = 0. \tag{3.14c,d}$$

Here, γ is chosen so that γU_1 is O(1) and $\gamma U_1 > \beta$ somewhere in the channel. Using a shooting method (e.g., Drazin and Reid 1981), we directly solved the eigenvalue problem (2.17a–c) with the solution of the form (3.7) being substituted, but with the nonlinear and the dispersive terms omitted. For the numerical solutions, we did not assume any truncation. Note that if U_2 is a constant, the following numerical results are directly applicable by replacing c and Δ by $c - U_2$ and $\Delta - U_2$, respectively.

Figure 7a shows the case where $r_1 = r_2 = 0$. The system is unstable for $0.05 < \Delta < 1.35$, which is consistent with the results obtained by Kubokawa (1989) and MG. Note that the phase speed of the U mode is smaller than Δ as $|\Delta| \to \infty$. This is consistent with c_U (3.8b) because the second term on the right-hand side of (3.8b) is always smaller than zero [see (3.6d)].

Figure 7b shows the case where $r_1/k = \gamma r_2/k = 0.1$. In this case $\mathrm{Im}(\lambda) = 0$ from (3.8b–d), so that we can expect the case 1 behavior of Fig. 6. Indeed, the real part of the phase speed indicates that there is an exchange of modes between the U mode and the L mode as Δ varies. Intersection of $\mathrm{Im}(c)$ between the two modes occurs as $\Delta \to \infty$ (or $-\infty$) because $\mathrm{Im}(\lambda^2 - \lambda_0^2) = 0$ only when $|\Delta| \to \infty$. In this case the bottom and interfacial friction are quite small, and therefore, the instability range is $0.05 < \Delta < 1.35$ again.

Figure 7c represents the case when $r_1/k = 0.1$ and $r_2 = 0$; only interfacial friction is considered. This shows the case 2 behavior of Fig. 6. Since $\gamma r_2 = 0$ in this case, we can see the widening of the instability range in terms of Δ as expected by the analytical solution (3.8). In fact, the system is apparently unstable for all $|\Delta|$.

Figure 7d shows the case when $r_1 = 0$ and $\gamma r_2/k = 0.1$; that is, only bottom friction is included. Com-

paring with the inviscid case, bottom friction widens the instability range, but in this case the system is unstable only for $\Delta > 0$, while the system is stable otherwise. In fact, if we substitute $r_1 = 0$ and $U_2 = 0$ into (3.8), we obtain

$$c = 0, \left(1 + \frac{b\gamma}{q_N^2}\right)q_N - \frac{i\gamma r_2}{k}, \quad \text{at} \quad \Delta = 0. \quad (3.15a)$$

This indicates that the instability range does not extend toward $\Delta \to -\infty$ beyond $\Delta = 0$ if only bottom friction is included. The eigenvalue $c = 0$ is interesting because it implies a stationary solution without growth or decay even though baroclinic energy conversion and frictional dissipation are included. In fact, if we substitute $r_1 = 0$, $U_2 = 0$, $\Delta = 0$, and (3.7) with $c = 0$ into (3.6a,b), then

$$B_X = 0, \quad q_N B_X + \gamma r_2 B = 0, \quad (3.15b)$$

and hence, the solution is $B = 0$. Therefore, the upper-layer motion is not affected by bottom friction, and there is no coupling between the two layers because $B = 0$.

Before concluding this section we examine the case of $\gamma^{1/2} \ll 1$ as this is the limit we shall take to study the weakly nonlinear theory in the next section. We define

$$\Delta = q_N + \gamma^{1/2}\Delta^{(1)}, \quad (3.16)$$

and replace r_1 with $\gamma^{1/2}r_1$, and γr_2 with $\gamma^{1/2}r_2$. The motivation of the scaling for r_2 is that we wish the effect of bottom friction to be comparable with that of interfacial friction. Then (3.8) reduces to $O(\gamma^{1/2})$

$$c = q_N + \gamma^{1/2}\left[\frac{\Delta^{(1)}}{2} - \frac{i}{2k}(r_1 + r_2)\right] \pm \frac{\gamma^{1/2}}{2}\sqrt{\lambda^2 - \lambda_0^2}, \quad (3.17a)$$

where

$$\lambda = \Delta^{(1)} - ik^{-1}(r_1 - r_2), \quad (3.17b)$$

$$\lambda_0^2 = -4b. \quad (3.17c)$$

When $b > 0$, there are the two cases for the asymptotic behavior in c as $\Delta^{(1)}$ varies, as in (3.10). If $b < 0$, however, there is only the case 2 behavior because the branch points are placed on the real axis of the λ-Riemann surface. If $r_1/k = r_2/k \ll 1$, (3.17a–c) show that

$$\text{Im}(c) = 0 \quad \text{at} \quad \Delta^{(1)} \approx \pm 2(-b)^{1/2}. \quad (3.18)$$

Thus, the inviscid result obtained by MG, in which $r_1 = \gamma r_2 = 0$ is a priori assumed, is recovered. Further, if either $r_1 \to 0$ and $r_2 \neq 0$ or $r_2 \to 0$ and $r_1 \neq 0$, then $\text{Im}(c) \to 0$ as $\Delta^{(1)} \to \infty$, so that the widening of the instability range due to differential friction between bottom and interface is also obtained even when $\gamma^{1/2} \ll 1$.

4. Baroclinic solitary wave in the presence of friction and multiple equilibria

In this section we will examine the evolution of an unstable solitary wave assuming $\gamma^{1/2} \ll 1$ in (2.17a–c). In this case, the coupling between the two layers is weak, that is, $O(\gamma^{1/2})$, and hence if friction is weak, (2.17) may reduce to a perturbed KdV equation as formulated in section 4a. The main purpose of this section is to demonstrate that there are multiple equilibria where baroclinic energy conversion and frictional dissipation are in balance by using a perturbation theory for KdV-type equations. This is discussed in section 4b, and the stability of the equilibria is examined in 4c.

a. Perturbation theory of a single solitary wave

We first introduce a time scale that is appropriate for the amplitude evolution due to weak baroclinic instability as follows:

$$\tau = \gamma^{1/2}T. \quad (4.1)$$

Further, as we did in the end of section 3, we replace r_1 and γr_2 with $\gamma^{1/2}r_1$ and $\gamma^{1/2}r_2$, respectively, so that the time scale due to interfacial and bottom friction is comparable to that due to baroclinic instability. Further, we expand ψ in powers of $\gamma^{1/2}$ so that

$$\psi = \gamma^{1/2}\psi^{(0)} + \gamma\psi^{(1)} + \cdots. \quad (4.2)$$

Then we obtain, to $O(\gamma^{1/2})$,

$$-(A_T + \Delta A_X) + 6AA_X + A_{XXX} - \gamma^{1/2}r_1 A + \gamma^{1/2}\int_{-L}^{0} U_1\psi_X^{(0)}dy = 0, \quad (4.3)$$

for the upper-layer motion. Hence, the leading-order part of (4.3) gives the KdV equation, which has a solitary wave solution of the form $A_s(\theta, \tau)$ where

$$A_s = a(\tau)\,\text{sech}^2 l\theta, \quad (4.4a)$$

where

$$\theta = X - \int_0^T c(\tau')dT', \quad (4.4b)$$

$$a = 2l^2. \quad (4.4c)$$

In (4.4b), c is a function of τ because c depends on the amplitude of the solitary wave, which changes owing to baroclinic instability and friction whose time scale is τ. Note that c in this section is real, so that c describes only the phase speed of the solitary wave. The growth rate is described by $\partial a/\partial\tau$. To solve (4.3) we appeal to perturbation theory (for instance, see Karpman and Maslov 1978; Kaup and Newell 1978; or Grimshaw and Mitsudera 1992). We may obtain a solution of the form

$$A = A_s + \delta A,$$

where δA is the correction to the solitary wave solution of $O(\gamma^{1/2})$, which arises due to the weak perturbation term in the KdV equation (4.3). The analysis is quite involved and we will not give details here, but the result may be simply described to $O(\gamma^{1/2})$ as follows:

$$\frac{da}{d\tau} = I_B - \frac{4}{3} r_1 a, \tag{4.5a}$$

$$c = \Delta - 2a + \gamma^{1/2}\left(J_B - \frac{r_1}{3l}\right), \tag{4.5b}$$

where

$$I_B = \int_{-\infty}^{\infty} \left(\int_{-L}^{0} \psi^{(0)} U_1 dy\right)_\theta \operatorname{sech}^2 z dz, \tag{4.5c}$$

$$J_B = \frac{1}{4l^3} \int_{-\infty}^{\infty} \left(\int_{-L}^{0} \psi^{(0)} U_1 dy\right)_\theta L(z) dz, \tag{4.5d}$$

$$L(z) = z \operatorname{sech}^2 z + \tanh z + \tanh^2 z, \tag{4.5e}$$

$$z = l\theta. \tag{4.5f}$$

Equation (4.5a) represents amplitude evolution, where the first term of the right-hand side describes amplification due to baroclinic instability, while the second term describes dissipation due to interfacial friction. Equation (4.5a) may be obtained directly by considering energy conservation or the upper layer. On the other hand, (4.5b) represents the phase speed of the solitary wave to $O(\gamma^{1/2})$, where J_B represents the coupling between the upper- and lower-layer motions. Note that (4.5b) reduces to Γ (1.2) if there is no coupling between the two layers and no interfacial friction (i.e., $\gamma^{1/2} \to 0$). We do not present δA here, as it is not necessary for the following discussion.

Here we suppose that a U mode solitary wave is almost resonant with the L mode. Then we may expand c as

$$c = q_N + \gamma^{1/2} c^{(1)} + \cdots, \tag{4.7}$$

where we recall that q_N is the phase speed of the L mode, that is, $\mathrm{Re}(c_L)$ as in (3.8c). Then we obtain

$$\psi^{(0)} = d_1^{-1} B(U_2 - q_N)\eta_N, \tag{4.8}$$

as the lowest-order solution, where B is the amplitude of the lower-layer motion and η_N satisfies the eigenvalue problem (3.2a,b). The next-order equation becomes, after applying the compatibility condition,

$$B_\tau - c^{(1)} B_\theta - b A_{s\theta} + r_2 B = 0. \tag{4.9}$$

Since θ (4.4b) is the reference frame moving with the solitary wave, $c^{(1)}$ in (4.9) may depend on τ. Substituting (4.8) into (4.5c,d), I_B and J_B reduce to

$$I_B = \int_{-\infty}^{\infty} B_\theta \operatorname{sech}^2 z dz, \tag{4.10a}$$

$$J_B = \frac{1}{4l^3} \int_{-\infty}^{\infty} B_\theta L(z) dz. \tag{4.10b}$$

Finally we may obtain the phase speed relationship to $O(\gamma^{1/2})$ from (4.5b) and (4.7), such that

$$q_N + \gamma^{1/2} c^{(1)} = \Delta - 2a + \gamma^{1/2}\left(J_B - \frac{r_1}{3l}\right). \tag{4.11}$$

Equation (4.11) implies that a may vary only $O(\gamma^{1/2})$ from the phase speed corresponding to exact resonance, which occurs when $a = a^{(0)}$, where

$$2a^{(0)} = \Delta - q_N. \tag{4.12a}$$

Thus, we may define the deviation of the amplitude from $a^{(0)}$ to be $a^{(1)}$ where

$$2a^{(1)} = -c^{(1)} + \left(J_B - \frac{r_1}{3l}\right). \tag{4.12b}$$

We have obtained a set of equations (4.5a), (4.9), (4.10a,b), and (4.12a,b) to describe the evolution of a single solitary wave. Note that since $a^{(0)} > 0$ it follows from (1.3) that $\Delta > \Gamma$. But the width of the linear instability zone with respect to Δ is only $O(\gamma^{1/2})$ since we are considering only the case $\gamma \ll 1$ here. Hence we shall suppose that the system is linearly stable here, and so $\Delta > \Gamma_2$.

b. Steady propagation—multiple equilibria

Here, we shall investigate steady propagation of a solitary wave, where a and c are constants and $\partial/\partial\tau \equiv 0$. Then, from (4.9), we obtain the lower-layer motion as follows:

$$B_\theta = -\frac{b}{c^{(1)}} A_{s\theta} - \frac{b r_2}{c^{(1)2}} \int^{\theta} A_{s\theta'} e^{(r_2/c^{(1)})(\theta-\theta')} d\theta'. \tag{4.13}$$

Equation (4.13) indicates that B is in phase with A_s if $r_2 = 0$. In this case, $I_B = 0$ from (4.10a), so that there is no baroclinic energy conversion. Thus, in order to maintain steady propagation, $r_1 = 0$ is necessary from (4.5a). This is the nonfrictional case, and such steady propagation is seen in Fig. 1b after the upper-layer solitary wave changes the direction. However, if $r_2 > 0$, B is no longer in phase with A_s, and thus, $I_B \neq 0$. That is, in order to propagate steadily, baroclinic energy conversion is required to balance the effects of bottom and interfacial friction.

Substituting (4.13) into (4.10a) we obtain

$$I_B = -\frac{a^2 b}{2r_2} \Omega(\alpha), \tag{4.14a}$$

where

$$\Omega(\alpha) = \frac{1}{\alpha^2} \int_{-\infty}^{\infty} \left[\int_{\pm\infty}^{z} (\operatorname{sech}^2 z')_{z'} e^{(1/\alpha)(z-z')} dz'\right] \times \operatorname{sech}^2 z dz, \tag{4.14b}$$

$$\alpha = c^{(1)} l / r_2, \tag{4.14c}$$

where $\pm$ as $\alpha \gtrless 0$. Note that $\Omega(\alpha) = \Omega(-\alpha)$. Asymptotic expressions of Ω as $\alpha \to \infty$ and $\alpha \to 0$ may be obtained by integrating the inside of the parenthesis [ ] of (4.14b) by parts, so that

$$\Omega(\alpha) \sim \frac{4}{3\alpha^2} + \cdots \quad \text{as} \quad \alpha \to \infty \tag{4.15a}$$

and

$$\Omega(\alpha) \sim \frac{16}{15} - \frac{64}{21}\alpha^2 + \cdots \quad \text{as} \quad \alpha \to 0. \tag{4.15b}$$

In Fig. 8 we display Ω, which was obtained by integrating (4.14) numerically. It shows that Ω has the maximum value $16/15$ at $\alpha = 0$ as in (4.15a) and decreases monotonically as $|\alpha|$ increases.

Further, we substitute (4.13) into (4.10b) and find

$$J_B = \frac{bl}{2r_2}\chi(\alpha), \tag{4.17a}$$

where

$$\chi(\alpha) = \frac{2}{\alpha} + \frac{1}{\alpha^2}\int_{-\infty}^{\infty}\left[\int^{z}(\operatorname{sech}^2 z')_{z'}e^{(1/\alpha)(z-z')}dz'\right]L(z)dz. \tag{4.17b}$$

Asymptotic expressions for $\chi(\alpha)$ are

$$\chi(\alpha) \sim \frac{2}{\alpha} - \frac{2}{3\alpha^2} + \cdots \quad \text{as} \quad \alpha \to \infty \tag{4.18a}$$

and

$$\chi(\alpha) \sim \frac{16}{15} + \frac{8\alpha}{3} + \cdots \quad \text{as} \quad \alpha \to 0. \tag{4.18b}$$

Note that for $r_1 = r_2 = 0$, which implies that $\alpha \to \infty$, (4.12b) and (4.18a) yield

$$2a^{(1)} = -c^{(1)} + \frac{b}{c^{(1)}}. \tag{4.19}$$

This is the linear solution (3.17a) but with $\Delta^{(1)}$ replaced by $-2a^{(1)}$. In fact, if we assume nonfrictional steady propagation a priori, Kubokawa and MG have shown that the phase speed of a coupled solitary wave corresponds directly to the linear one where Δ is replaced by $\Gamma = \Delta - 2a$. Noting that $-2a^{(1)}$ is the $O(\gamma^{1/2})$-term of Γ, (4.19) recovers the result of Kubokawa and MG, and hence, the perturbation theory developed here reproduces this coupling effect correctly.

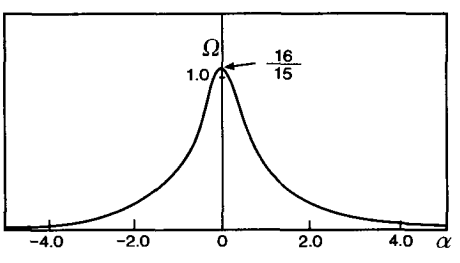

FIG. 8. Plot of Ω as a function of α.

Now we may obtain equilibria in terms of the amplitude. From (4.3), (4.4a), and (4.9) we first realize that $a = 0$ and $B = 0$ are trivial solutions. Next, assuming $a \neq 0$, we define

$$\rho = -\frac{8r_1r_2}{3ab}. \tag{4.20a}$$

Then we may see from (4.14a) that (4.5a) (without a_τ) has solutions if

$$\rho = \Omega(\alpha) \tag{4.20b}$$

is satisfied. Since $0 < \Omega \leqslant 16/15$ (see Fig. 8), we have two equilibria when

$$0 < \rho \leqslant \frac{16}{15}. \tag{4.21}$$

If $\rho < 0$ or $\rho > 16/15$, there is no steady state except for $a = 0$. If $\rho = 0$, there are two solutions if $r_1 = r_2 = 0$, while if either of r_1 or r_2 is not zero, there are no steady solutions within the range where the perturbation theory with $\gamma^{1/2} \ll 1$ is valid [see (4.23) below]. Note that $\rho \gtrless 0$ when $b \lesseqgtr 0$. Therefore, multiple equilibria is realized only when $b < 0$, that is, when the basic current has an unstable configuration. In this case, therefore, weak bottom friction and weak interfacial friction tend to cause the multiple equilibria. In contrast, if $b > 0$, the solitary wave has only one equilibrium where the amplitude of the solitary wave is zero.

We have so far obtained α from (4.20b), which in turn gives $c^{(1)}$ from (4.14c). The amplitude variation is then obtained by (4.12b). If we suppose that the two solutions for (4.20b) are $\alpha = \pm\alpha_e$, the equilibrium with the larger amplitude $a_+^{(1)}$ (the smaller amplitude $a_-^{(1)}$) is represented by $-\alpha_e$ (α_e).

For further understanding, we display a schematic plot of the bifurcation diagram in Fig. 9, where

$$a_\pm = a^{(0)} + \gamma^{1/2}a_\pm^{(1)}.$$

When $r_1, r_2 \ll 1$ and $c^{(1)} = O(1)$, which implies $\alpha \gg 1$, we obtain, from (4.15a) and (4.20a),

$$c^{(1)2} = -b\frac{r_2}{r_1}. \tag{4.22}$$

Thus, using (4.12) and (4.19a), and again considering $r_1, r_2 \ll 1$, we obtain multiple equilibria such that

$$2a_\pm^{(1)} = \pm\sqrt{-b}\left[\left(\frac{r_1}{r_2}\right)^{1/2} + \left(\frac{r_2}{r_1}\right)^{1/2}\right]. \tag{4.23}$$

Therefore,

$$a_\pm^{(1)} = \pm(-b)^{1/2} \quad \text{when} \quad r_1 = r_2, \tag{4.24a}$$

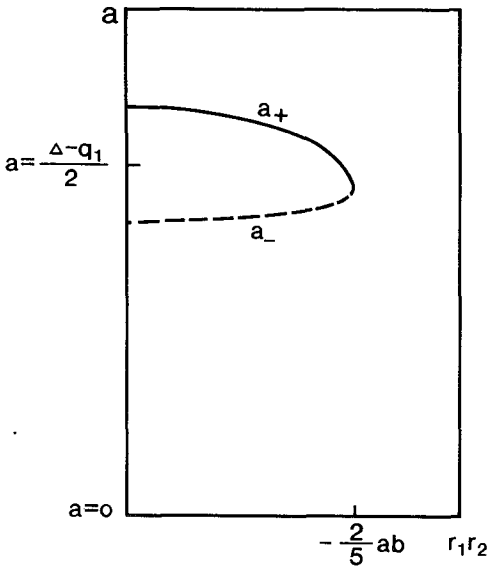

FIG. 9. Schematic plots of the bifurcation diagram. Solid lines with $a = a_+$, 0 denote stable branches, while a dashed line with $a = a_-$ denotes an unstable branch.

while

$a_\pm^{(1)} \to \pm\infty$ when either

$$r_1 \to 0 \quad \text{only or} \quad r_2 \to 0 \quad \text{only.} \tag{4.24b}$$

Equation (4.24a) is identical to (3.17a) if $-2a^{(1)}$ is replaced with $\Delta^{(1)}$, as expected by the discussion below (4.19).

When $r_1 r_2$ increases, which implies that ρ increases, then $|\alpha|$ decreases as seen in Fig. 8. When ρ equals $16/15$, there is a single solution, $\alpha = 0$ (or $c^{(1)} = 0$). Just below this point, we obtain from (4.12) and (4.18b)

$$2a_\pm^{(1)} \approx \frac{8bl}{15r_2} - \frac{r_1}{3l} \mp \alpha_e \frac{r_2}{l}\left(1 + \frac{5r_1}{4r_2}\right) + O(\alpha_e^2), \tag{4.25a}$$

so that we confirm there are two solutions for $\rho < 16/15$. If $r_1 r_2$ further increases, (4.20b) no longer has solutions.

c. *Time dependent solution and stability of equilibria*

Next, we shall investigate the evolution of a solitary wave with time. From (4.9) we obtain the lower-layer motion as follows:

$$B = b\int_0^\tau e^{-r_2(\tau-\tau')} A_{s\theta}\left(\theta + \int_{\tau'}^{\tau} c^{(1)}(\tau'')d\tau'', \tau'\right)d\tau'. \tag{4.26}$$

Substituting (4.26) into (4.10a) and (4.10b) we obtain

$$I_B = -\frac{b}{2}\int_0^\tau e^{-r_2(\tau-\tau')}\, a^2(\tau')\Pi(S)d\tau', \tag{4.27a}$$

$$J_B = \frac{b}{8l^3}\int_0^\tau e^{-r_2(\tau-\tau')}a^2(\tau')\Phi(S)d\tau', \tag{4.27b}$$

where

$$\Pi(S) = -\int_{-\infty}^{\infty} (\operatorname{sech}^2 z)_{zz} \operatorname{sech}^2(z+S)dz, \tag{4.27c}$$

$$\Phi(S) = \int_{-\infty}^{\infty} L_{zz} \operatorname{sech}^2(z+S)dz, \tag{4.27d}$$

and

$$S(\tau, \tau') = l(\tau')\int_{\tau'}^{\tau} c^{(1)}(\tau'')d\tau''. \tag{4.27e}$$

We note here $\Pi(S) = \Pi(-S)$, $\Pi(0) = 16/15$, $\Pi \to 0$ as $S \to \infty$, and $\Phi(0) = 16/15$, $\Phi(0) \to 0$ as $S \to \infty$. In general, (4.27a,b) show that I_B and J_B are complicated functionals of a. But note that whenever $\Pi(S) > 0$, $I_B \gtrless 0$ according to $b \lesseqgtr 0$, and hence from (4.5a) the amplitude of the solitary wave decreases with time whenever $b > 0$, while the solitary wave can be unstable if $b < 0$, depending on the relative magnitudes of I_B and $4/3 r_1 a$ on the right-hand side of (4.5a). Considering the unstable case ($b < 0$) we can now anticipate that when $\Pi(S) < 0$, solitary waves will stabilize. In fact, $\Pi(S)$ is positive for $0 \leqslant |S| < 1.072$ and negative for $1.072 < |S| < \infty$. Therefore, solitary waves are stabilized for sufficiently large amplitudes even when there is no friction, as seen in Fig. 1b.

Friction determines the asymptotic behavior of the solitary wave as $\tau \to \infty$. We first suppose there is an asymptotic solution $a \to a_\infty$ and $c \to c_\infty$ as $\tau \to \infty$. Then we obtain, from (4.27e),

$$S \to lc_\infty(\tau - \tau'), \tag{4.28}$$

as $\tau \to \infty$. Thus, I_B becomes

$$\begin{aligned} I_B &\sim -\frac{ba^2}{2}\int_0^\infty \Pi(lc_\infty(\tau-\tau'))e^{-r_2(\tau-\tau')}d\tau' \\ &= -\frac{ba^2}{2lc^{(1)}}\int_0^{\pm\infty} \Pi(\zeta)e^{-\zeta/\alpha}d\zeta \\ &= -\frac{ba^2}{2r_2}\Omega(\alpha). \end{aligned} \tag{4.29a}$$

Similarly, J_B becomes

$$\begin{aligned} J_B &\sim \frac{bl}{2}\int_0^\infty \Phi(lc_\infty(\tau-\tau'))e^{-r_2(\tau-\tau')}d\tau' \\ &= \frac{bl}{2r_2}\chi(\alpha). \end{aligned} \tag{4.29b}$$

Since (4.29a) and (4.29b) are identical to (4.14a) and (4.17a), respectively, a asymptotically approaches a_∞, which is either a_+, a_-, or 0.

To determine which equilibrium value a approaches, we need to investigate the stability of these equilibria.

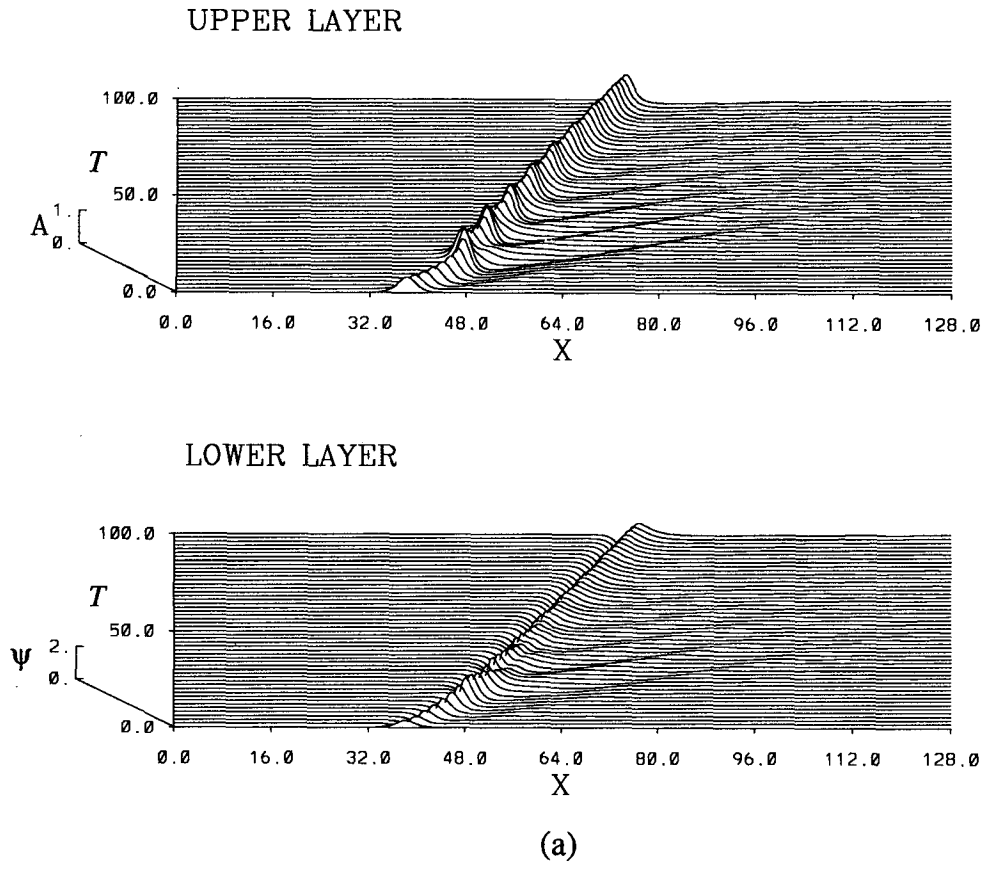

FIG. 10. Example of multiple equilibria from different initial amplitude, $a(0)$, obtained by numerical integration of (2.17) with (3.13) and (3.14). The other parameters are $\Delta = 1.6$, $r_1 = \gamma r_2 = 0.1$; (a) $a(0) = 0.5$, and (b) $a(0) = 0.4$.

First we consider $a_\pm$. We perturb a and $c^{(1)}$ such that $a \to a + \delta a$ and $c^{(1)} \to c^{(1)} + \delta c^{(1)}$, but here we note that from (4.11) the perturbation in a is only $O(\gamma^{1/2}\delta c^{(1)})$. Thus, the dominant term in (4.5a) is due to $\delta c^{(1)}$, so that

$$\frac{\partial}{\partial \tau}\delta a = \delta I_B + O(\gamma^{1/2}), \tag{4.30a}$$

where

$$\delta I_B = -\frac{ba^2}{2}\int_0^\infty \Pi'(S)e^{-r_2(\tau-\tau')}\delta S ds' + O(\gamma^{1/2}), \tag{4.30b}$$

$$\delta S = \delta c^{(1)} l(\tau - \tau'), \tag{4.30c}$$

and here Π' denotes the derivative. Thus we obtain

$$\delta I_B \sim -\frac{l}{r_2}\left(\frac{ba^2}{2r_2}\right)\delta c^{(1)}\Omega'(\alpha) \tag{4.31a}$$

$$= \frac{\partial I_B}{\partial c^{(1)}}\delta c^{(1)}. \tag{4.31b}$$

Equation (4.31b) indicates that the system is quasi-steady as $\tau \to \infty$, at least for $\gamma^{1/2} \ll 1$, even though we have included the B_τ term in the lower-layer equation (4.9). Hence we have, from (4.5a) and (4.30a),

$$\frac{\partial}{\partial \tau}\delta a \sim \frac{\partial I_B}{\partial c^{(1)}}\delta c^{(1)}. \tag{4.32}$$

Next, from (4.5b) we obtain

$$2\delta a^{(1)} = -\delta c^{(1)} + \delta J_B + O(\gamma^{1/2}). \tag{4.33}$$

Here, noting that variation in J_B is due to $\delta c^{(1)}$ alone to the lowest order, we obtain

$$\delta J_B \sim \frac{bl^2}{2r_2^2}\chi'(\alpha)\delta c^{(1)}. \tag{4.34}$$

However, from the steady solution (4.12b) we obtain

$$2\frac{\partial a^{(1)}}{\partial c^{(1)}} = -1 + \frac{bl^2}{2r_2^2}\chi'(\alpha). \tag{4.35}$$

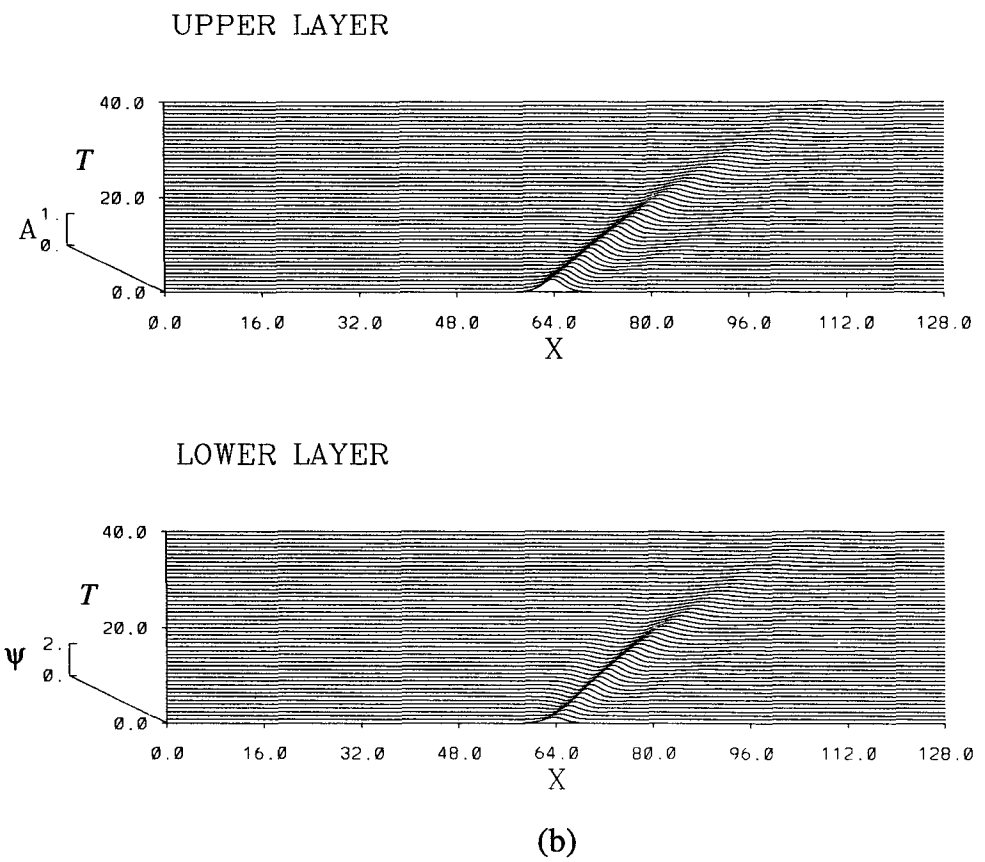

(b)

FIG. 10. (*Continued*)

Substituting (4.34) and (4.35) into (4.33) we finally obtain

$$\delta a^{(1)} \sim \frac{\partial a^{(1)}}{\partial c^{(1)}} \delta c^{(1)}. \tag{4.36}$$

This again indicates that the system is quasi steady. Now, from (4.31), (4.32), and (4.36), and noting that generally $\partial\alpha/\partial a^{(1)} < 0$, we obtain that the system is stable if $\Omega'(\alpha) > 0$, while unstable if $\Omega' < 0$. Therefore, from Fig. 9, $-\alpha_e$ (α_e) is stable (unstable), but since $-\alpha_e(\alpha_e)$ represents a_+ (a_-), we have finally found that

- a_+ is stable,
- a_- is unstable.

This conclusion can possibly be reversed if r_2 is sufficiently small and r_1 simultaneously sufficiently large so that for some small range of values of α, $\partial\alpha/\partial a^{(1)} > 0$; however, we shall assume this does not occur here.

To determine the stability of $a = 0$ we appeal to the linearized theory and recall from the discussion at the end of section 4a that here the linearized system is stable. Hence we conclude that $a = 0$ is stable, at least for $\gamma^{1/2} \ll 1$.

d. Brief summary

In summary we have obtained two stable equilibria, $a = a_+, 0$, and an unstable equilibrium, $a = a_-$ when $b < 0$ and ρ (4.20a) lies between 0 and $^{16}/_{15}$. Therefore, a solitary wave with $a > a_-$ approaches asymptotically a_+, while one with $a < a_-$ decays to zero. In particular, if $a_- < a < a_+$, baroclinic energy conversion exceeds frictional dissipation, so that localized baroclinic instability occurs. Figure 9 summarizes the result of this section, where the stable branches (i.e., $a = a_+, 0$) are denoted by solid lines, and the unstable branch (i.e., $a = a_-$) by a dashed line. From (4.24b), $a_\pm^{(1)} \to \pm\infty$ when either $r_1 \to 0$ and $r_2 \neq 0$, or $r_2 \to 0$ and $r_1 \neq 0$. Therefore, we have found that differential friction between the bottom and the interface destabilizes solitary waves as well. This is because friction tends to produce phase difference between the two layers [e.g., see (4.13)], which then induce baroclinic energy conversion. Hence if either friction term vanishes, the energy conversion cannot be balanced, leading to instability. This result is consistent with that of the linear stability analysis discussed in section 3.

To reiterate the conclusion in this section is valid

for $\gamma^{1/2} \ll 1$ and $a^{(0)} = O(1)$. Further, we considered coupling only with a single lower-layer mode. In section 5, we will discuss the results of direct numerical integrations of (2.17), which is free from the above restrictions. Finally, note that in the Appendix we discuss the energetics of the instability processes discussed here.

5. Numerical results

To investigate the evolution of solitary waves and the multiple equilibria free of the restrictions of the perturbation theory of section 4, we performed numerical integrations of (2.17) directly using a pseudospectral method (i.e., obtaining X derivatives using Fourier transform) similar to that developed by Fornberg and Whitham (1978). In the lower layer, we used a finite-difference scheme in the y coordinate with the number of grids being 21. Note that only a single cross-channel mode is generated. The channel width is $L = 2$. The upper current $U_1(y)$, the depth ratio γ, meridional gradient of Coriolis parameter β, and the lower current U_2 are the same as (3.13) and (3.14a–d), respectively, in the figures to be displayed. Calculations are performed in the domain $0 \leq X \leq 128$, where a damping layer is put in $0 \leq X \leq 24$ so that the calculations are not affected by the periodic condition of the pseudospectral method. Note that upstream is $X \to -\infty$ here. In all cases the lower-layer plots are for $\psi(y = -1)$. We shall describe the behavior of solitary waves in three cases separately, where $r_1 = \gamma r_2 \neq 0$ (Case 1), $r_1 = 0$, $r_2 \neq 0$ (Case 2), and $r_1 \neq 0$, $r_2 = 0$ (Case 3), since the behavior is greatly different for these cases.

a. *Case 1: $r = r_1 = \gamma r_2$*

In this subsection, both bottom friction and interfacial friction are included. Further, we assume $r_1 = \gamma r_2 = r$ because this is a typical situation where both types of friction are considered. The nonfrictional case is a special case of this assumption.

In Figs. 10a and 10b we display an example of multiple equilibria attained by different initial conditions. For both these cases, $\Delta = 1.6$ and $r_1 = \gamma r_2 = 0.1$. Figure 10a shows that if $a(0) = 0.5$, where $a(0)$ denotes a at $T = 0$, the solitary wave in the upper layer grows initially and shows an oscillatory behavior. However, it attains a steady state as $\tau \to \infty$, with $a \approx 0.8 (= \Delta/2)$ and propagates steadily downstream. This is the large amplitude state, and hence, $a_+ \approx 0.8$ in this system. From Fig. 10a baroclinic energy conversion is evident because the lower-layer motion has a depression upstream and an elevation downstream with respect to the upper-layer solitary wave when it becomes steady. This is the desirable phase relation for localized baroclinic instability to occur [see (A1a)]. On the other hand, if $a(0) = 0.4$, baroclinic instability does not occur as shown in Fig. 10b, and hence the solitary wave decays to zero, which is the other steady state of this system. Hence, for $r_1 = \gamma r_2 = 0.1$, we have obtained two stable steady states where $a \approx 0.8$ and $a = 0$, and an unstable equilibrium somewhere between $a = 0.4$ and 0.5. This is consistent with the perturbation analytical solution discussed in section 4.

In Fig. 11, we display a bifurcation diagram of a with respect to $r = r_1 = \gamma r_2$. The rest of the parameter values are the same as those for Figs. 10a and 10b. Since $\Delta = 1.6$, the system is stable for infinitesimal disturbances (i.e., linearly stable) if $r = 0$ (see Fig. 7a). Hence, there is a correspondence with the perturbation study in section 4, and features are similar to those in Fig. 9, in general. That is, there are three equilibria, $a = a_\pm$ and 0, for $0 < r < 0.18$, while there is one equilibrium, $a = 0$, for $r > 0.18$. For $0 < r < 0.18$, a_- is always unstable, so that a solitary disturbance grows if $a_+ > a > a_-$, and decays if $a < a_-$. Further, $a = 0$ is the steady equilibrium that is stable for all r if $\Delta = 1.6$.

However, contrary to the results in section 4 where $\gamma^{1/2} \ll 1$, direct numerical calculations show that a_+ is not always stable if r is small enough, but the solitary wave shows an oscillatory behavior as $T \to \infty$. In this case the amplitude is oscillating about $a_+ \approx 0.8$. We display an example in Fig. 12a where $a(0) = 0.4$ and $r = 0.05$. A solitary wave grows due to baroclinic instability when it propagates downstream, while it de-

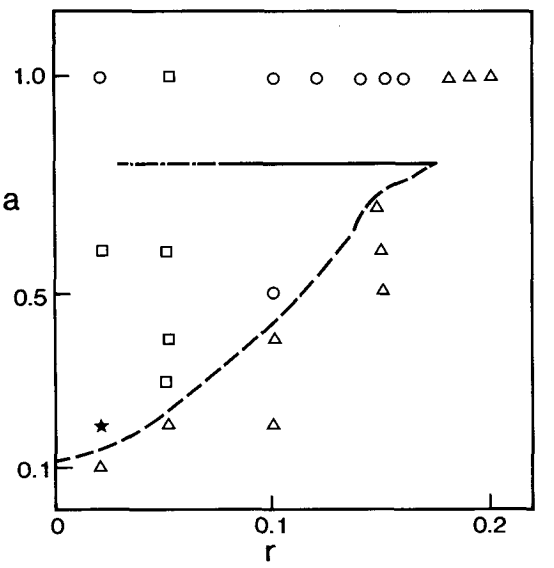

FIG. 11. Bifurcation diagram obtained by numerical integration of (2.17). Solid line indicates the stable branches, a_+ and 0, while dashed line indicates the unstable equilibrium, a_-. Dashed-dotted line indicates the part of a_+ where the solitary wave shows oscillatory behavior. Symbols indicate initial amplitudes, where each symbol means a different final state as follows. ○: steady propagation with $a = a_+$; △: $a = 0$; □: oscillation about a_+; ★: continuous generation of upper-layer solitary waves.

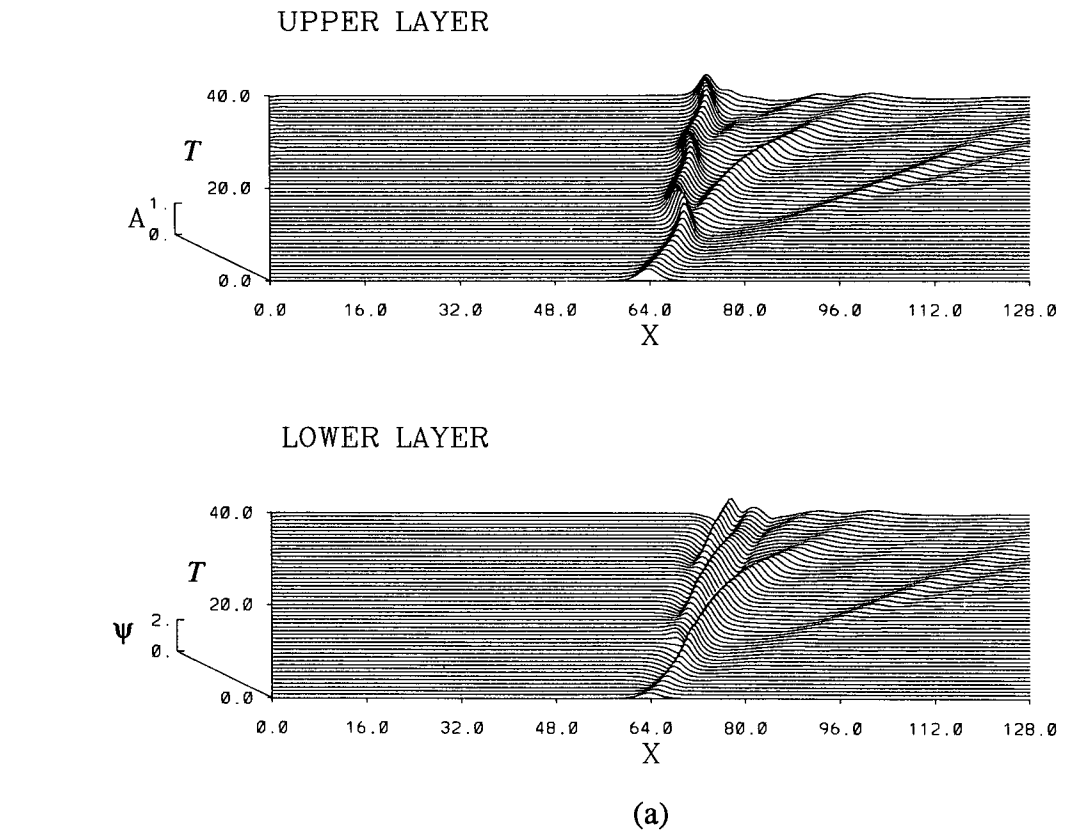

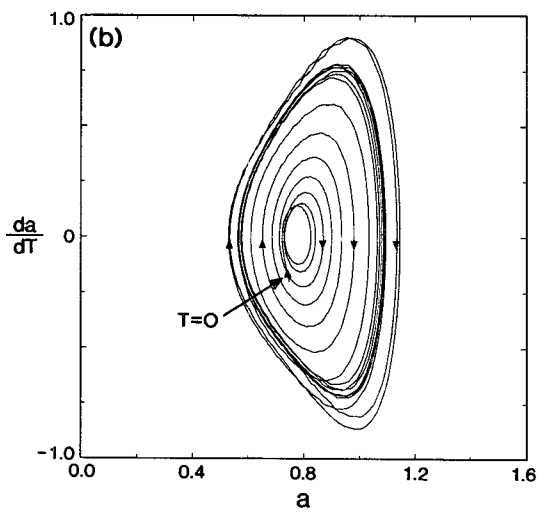

FIG. 12. (a) As in Fig. 10 except for $r_1 = \gamma r_2 = 0.05$ and $a(0) = 0.4$. (b) A phase diagram on $a - \partial a/\partial T$ plane; $a(0) = 0.75$.

cays when it propagates upstream due to friction. It changes direction when the amplitude passes $a = a_+ \approx 0.8$. Lower-layer waves are successively generated when the upper-layer solitary wave propagates downstream, which in turn provides strong coupling between the two layers so that the solitary wave grows. However, the lower-layer waves do not change direction because they are linear waves, and therefore, the coupling becomes weaker after the upper-layer solitary wave changes direction. Finally the lower-layer waves decay due to friction. The oscillatory behavior may be more clearly seen in phase diagrams. We display a phase diagram in terms of the amplitude and its time derivative in Fig. 12b, where the initial amplitude is $a(0) = 0.75$. This indicates that the equilibrium $a_+ \approx 0.8$ is unstable for $r = 0.05$ because the cycle grows with time. But

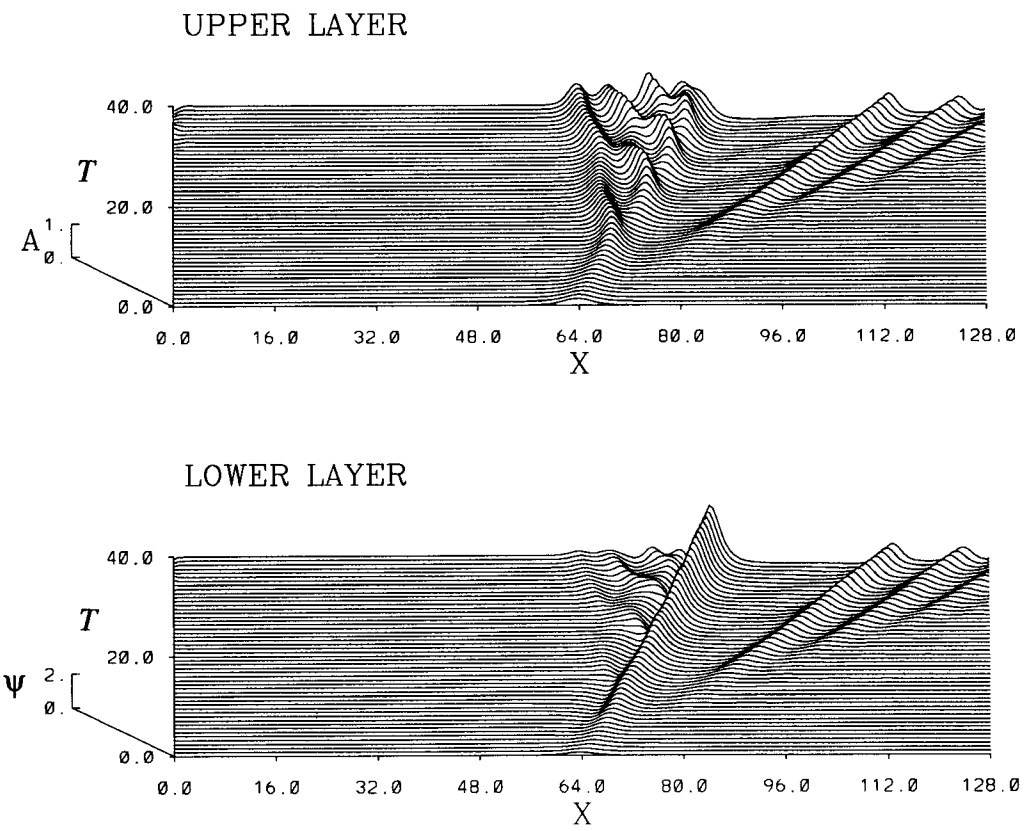

FIG. 13. As in Fig. 10 except for $r_1 = \gamma r_2 = 0.02$ and $a(0) = 0.2$.

finally it reaches a quasi-steady cycle where the trajectory is concentrated. The behavior is similar to that caused by a Hopf bifurcation.

When r_1 and γr_2 further decrease, baroclinic instability dominates frictional dissipation. Therefore, the upper-layer solitary waves are generated upstream continuously from the unstable region and show complicated behavior because of wave–wave interactions. An example is shown in Fig. 13, where $r = 0.02$ and $a(0) = 0.2$. The behavior of this case is similar to that of inviscid cases such as that in Fig. 1b, although the upper-layer waves decay weakly due to friction.

If the system is linearly unstable for $r = 0$, the equilibrium $a = 0$ could be unstable for small r. To test this hypothesis, we performed numerical calculations with $\Delta = 1.0$, which is certainly in the linearly unstable range if $r = 0$ (see Fig. 7a). The consequent bifurcation diagram is displayed in Fig. 14. It shows that characteristics are similar to Fig. 11 in general; for example, $a_+ \approx 0.5$ exists for $r < 0.17$. Note that even if r is small, a solitary wave with sufficiently small amplitude is likely to be stable. Therefore, $a = 0$ is likely to be a stable branch for $r > 0$ even when Δ is in the linearly unstable range for $r = 0$. For example, the solitary wave with $a = 0.01$ is stable for $r = 0.02$. The analysis in section 4 is suggestive of this character, although it is valid only for $\gamma^{1/2} \ll 1$. That is, ρ (4.20a) increases as a decreases, so that if a becomes sufficiently small, ρ goes out of range of instability for any $r \neq 0$. In fact, if $a \ll 1$, the linear stability analysis in section 3 may be appropriate. If we use an initial disturbance of the form (4.4a), energy is concentrated on very small wavenumbers k if a is small because the half-width l is proportional to $a^{-1/2}$. Therefore, r/k is, on average, large for such initial disturbance. From the linear analysis in section 3 [e.g., see (3.8)], the growth rate $\mathrm{Im}(kc)$ is negative and finite as $k \to 0$, so that frictional effects can be large even if r itself is small.

b. *Case 2: $r_1 = 0$ and $r_2 \neq 0$*

Here we consider cases in which only bottom friction is included. The corresponding linear stability diagram is Fig. 7d. In Fig. 15, we display an example where $r_1 = 0$, $\gamma r_2 = 0.1$, and $\Delta = 1.6$. The solitary wave grows and turns direction at $a \approx 0.8$ as in the previous cases. As $T \to \infty$, however, the upper-layer solitary wave becomes stationary; that is, $c \to 0$ and $a_T \to 0$. Therefore, there is a stable equilibrium a_+ in this situation. This is seemingly contradicting to the result of section

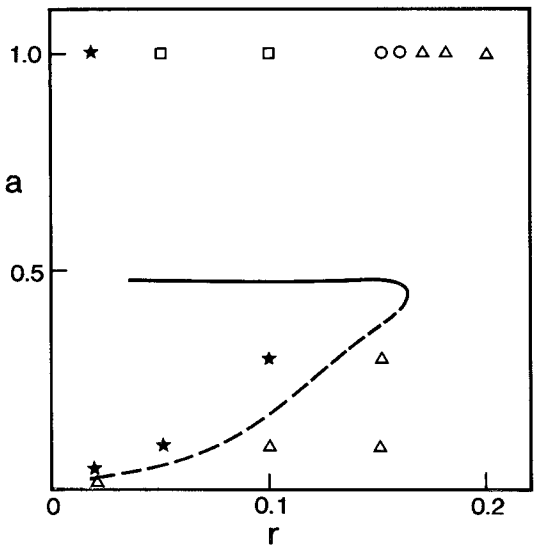

FIG. 14. The bifurcation diagram for $\Delta = 1.0$. The parameter values are (3.13) and (3.14), and the meanings of symbols are the same as Fig. 11.

4, which suggests that there is no steady state if $r_1 = 0$ and $r_2 \neq 0$ because $a_{\pm}^{(1)}$ (4.23) $\rightarrow \pm\infty$. But they are not contradictory at all, because the equilibrium at $c = 0$ is out of the range of validity of the perturbation theory, which assumes $\gamma^{1/2} \ll 1$. Actually, having a stationary solution corresponds directly to the characteristics of the linear stability of this system such that $c_r = c_i = 0$ at $\Delta = 0$ (see Fig. 7d). Further, the lower-layer motion accompanied by the solitary wave disappears as $T \rightarrow \infty$. This is consistent with the linear stability result in section 3 [see (3.15b)]. Therefore, the upper-layer motions are not affected by bottom friction as $T \rightarrow \infty$, so that the stationary state can be achieved when $U_2 = 0$. Further, a_+ is exactly $\Delta/2$ for this stationary solitary wave because $c = 0$, $r_1 = 0$, and $J_B = 0$ in (4.5b). Note that as the wave stabilizes and becomes stationary a second unstable wave is generated that also grows and stabilizes.

In Fig. 16, we display a strong bottom-friction case where $\gamma r_2 = 1.0$ and $r_1 = 0$. The initial amplitude $a(0) = 0.1$ and the rest of parameters are the same as those for Fig. 15. We have found that even though bottom friction is strong, the solitary wave is destabilized. This is seemingly puzzling, but is indeed expected by the discussion in section 4. That is, from (4.24b), the margin of instability $a_{\pm}^{(1)} \rightarrow \pm\infty$ for any value of bottom friction as long as interfacial friction is absent, and hence, instability occurs for even strong bottom friction. Further, it is noteworthy that the disturbance with $a(0) = 0.1$ is destabilized. Since in the nonfrictional

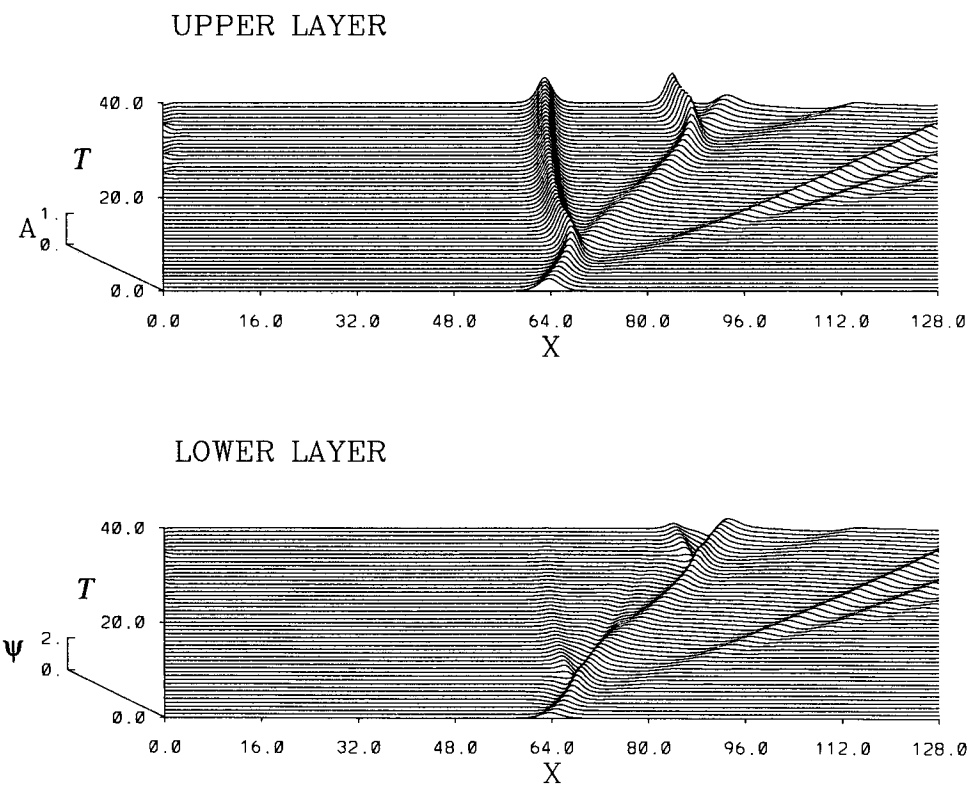

FIG. 15. As in Fig. 10 except for $r_1 = 0$, $\gamma r_2 = 0.1$, and $a(0) = 0.4$.

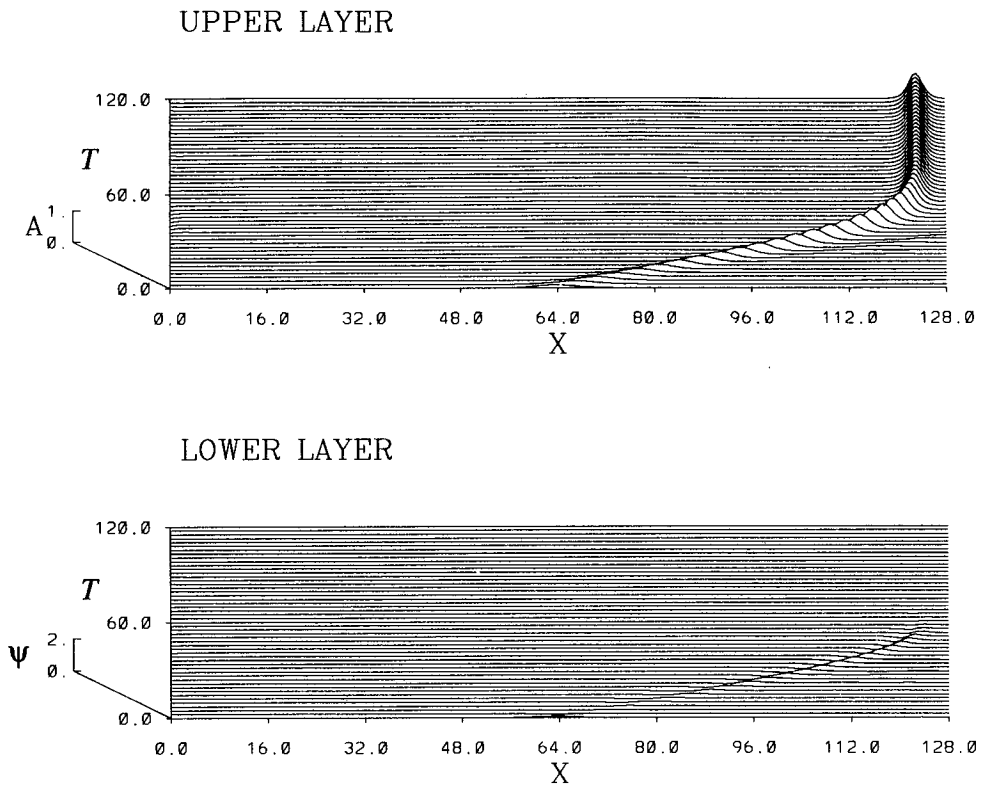

FIG. 16. As in Fig. 10 except for $r_1 = 0$, $\gamma r_2 = 1.0$, and $a(0) = 0.1$.

case, a solitary wave with $a = 0.1$ is stable (see Fig. 11), this confirms the widening of the instability range due to bottom friction as discussed in section 4. This is also consistent with the result of the linear instability analysis in section 3. We further performed a numerical calculation for $a(0) = 0.05$ and it also shows instability. In conjunction with the linear analysis, which indicates that the system is unstable for $\Delta \to +\infty$, $a = 0$ is likely to be an unstable branch and hence, there is probably only one stable equilibrium if interfacial friction is absent. This is because r_2 causes phase shift between the upper- and lower-layer motions [see (4.13)], which in turn causes baroclinic energy conversion; hence, if $r_1 = 0$, the balance (4.15) with $\partial a/\partial \tau = 0$ is achieved only if lower-layer motions vanish, which occurs when $c = 0$. In other words, both interfacial and bottom friction are necessary in order to obtain *two* stable equilibria.

c. *Case 3: $r_1 \neq 0$ and $r_2 = 0$*

Finally, we discuss the case where only interfacial friction is present. Figure 17 shows an example in which $\Delta = 1.6$, $r_1 = 0.05$, $\gamma r_2 = 0$, and $a(0) = 0.4$. In this case, the lower-layer motion is strongly unstable (e.g., compare with Fig. 14), generating upper-layer solitary waves continuously. Hence, there is no steady single solitary wave, as suggested by the perturbation theory in section 4. The upper-layer solitary wave, propagating upstream, decays as indicated by linear analysis (Fig. 7c) but shows complicated behavior due to wave–wave interactions.

6. Summary and discussions

In this paper we have described a weakly nonlinear theory of localized baroclinic instability where bottom and interfacial friction are included. Our main aim has been to show that there are multiple equilibria for solitary waves, where energy conversion due to baroclinic processes and frictional dissipation are in balance. We use a two-layer model, which consists of a thin upper layer and a deep lower layer; although the lower layer is deep, it is not stagnant, and hence, baroclinic instability can occur. Considering the weakly nonlinear, long-wave limit, we have shown that an evolution equation of the KdV type (2.17a) describes the upper-layer motion, with additional terms describing the coupling between the two layers, and interfacial friction. The lower-layer motion is described by a linear long-wave equation (2.17b,c) including bottom and interfacial friction, which is in turn coupled with the upper layer.

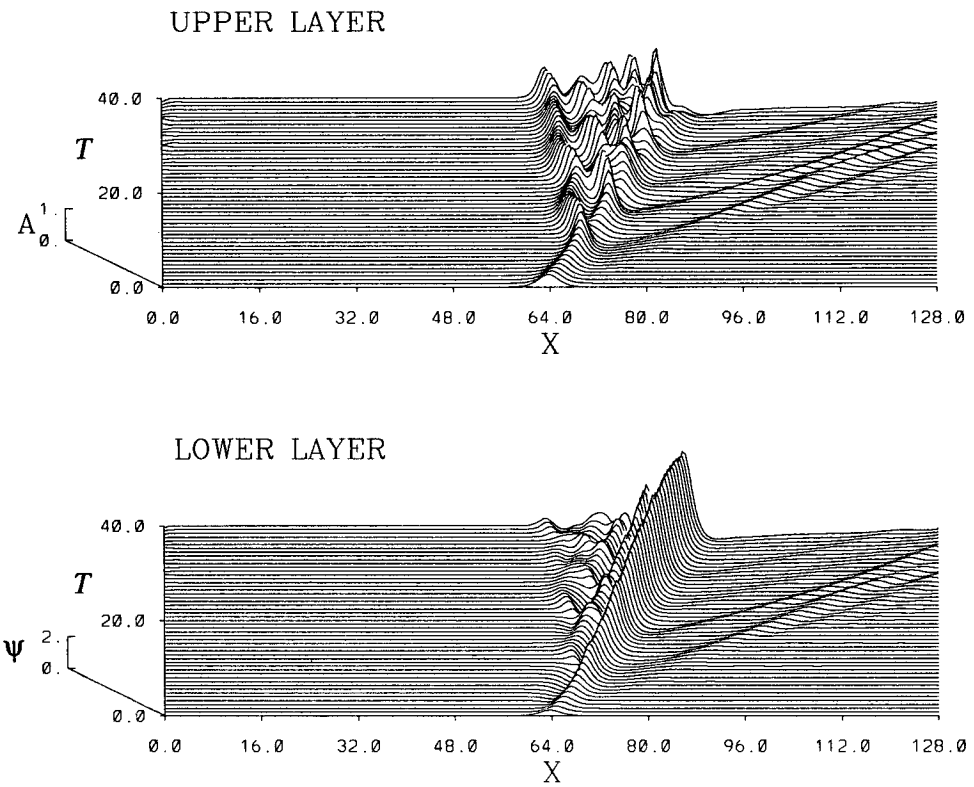

FIG. 17. As in Fig. 10 except for $r_1 = 0.05$, $\gamma r_2 = 0$, and $a(0) = 0.4$.

Before investigating the weakly nonlinear problem, we first solved a linear eigenvalue problem including bottom and interfacial friction, omitting the nonlinear and dispersive terms from the upper-layer equation [e.g., see (3.4)]. The results are summarized in Fig. 4 for b (3.5d) > 0, and in Fig. 6 for $b < 0$, where b represents the sign of the lower-layer potential vorticity gradient; a negative b indicates that the signs of the potential vorticity gradient of the two layers are opposite, and hence the basic current may be baroclinically unstable. Further, some typical cases of the eigenvalue problem are calculated numerically, and the results are displayed in Figs. 7a–d. An interesting consequence is that when the mean current has an unstable configuration (i.e., $b < 0$), differential friction between bottom and interface may enhance instability in a range where the system is stable for nonfrictional cases. This somewhat puzzling feature of the two-layer model was first found by Holopainen (1961) with bottom friction. Our study has proved that it persists into the long-wave limit. Further, we discussed this feature for the nonlinear case using energetic equations in the Appendix. This destabilizing effect of friction is most evident when either bottom or interfacial friction vanishes (see Figs. 7c,d, comparing with Fig. 7a).

The evolution of nonlinear, localized disturbances was then investigated analytically (section 4) and numerically (section 5). It has been found that there are multiple equilibria where baroclinic energy conversion and frictional dissipation are in balance. The multiple equilibria occurs when $b < 0$, and when $r_1 r_2$ is less than the critical value defined by (4.19a) and (4.20), where r_1 and r_2 are the (scaled) interfacial and bottom friction coefficients, respectively. If this criterion is satisfied, there are typically three equilibria for small but nonzero r_1 and r_2. In terms of the solitary wave amplitude, a, we obtained $a = a_+$, a_-, and 0 as the equilibria, where $a_+ > a_- > 0$. The equilibrium $a = a_-$ is unstable, and hence, a solitary wave with $a > a_-$ attains the large amplitude state $a = a_+$ as $T \to \infty$, while a solitary wave with $a < a_-$ decays to zero. In particular, if $a_+ > a > a_-$, baroclinic energy conversion exceeds frictional dissipation, and thus, localized instability occurs. But a_+ may also be unstable if friction is small enough; in this case, an upper-layer solitary wave shows oscillatory behavior, where the amplitude is oscillating about $a = a_+$.

If only bottom friction is included ($r_1 = 0$, and $r_2 > 0$), the system is unstable for any r_2 even if r_2 is large. Further, $a = 0$ is likely to be unstable. This is because r_2 causes a phase difference between the upper- and lower-layer motions [e.g. (4.13)], which in turn enhances baroclinic conversion; hence the solitary wave is unstable except when the lower-layer motion van-

ishes. Therefore, there is only the one stable equilibrium, a_+, in which the upper-layer wave has exactly zero phase speed (if the lower-layer current is absent). On the other hand, if only interfacial friction is included, solitary waves are continuously generated in the unstable region, and hence, there is no steady state. Therefore, in order to obtain multiple *stable* equilibria (i.e., $a = 0, a_+$) in a two-layer model, neither bottom friction nor interfacial friction should be zero.

One possible application of this study is to the behavior of the Kuroshio Current off the south coast of Japan. It is well known that the Kuroshio has two major paths; one is the straight path and the other is the large meander. Both of these paths are very stable, persisting for a few years, but transition from the straight paths to the large meander occurs rather quickly, that is, within three or four months. This indicates multiple equilibria of the Kuroshio system. Further, preceding the formation of the large meander, a "small meander" is generated off the coast of Kyushu (the westernmost part of Japan). It has been suggested from observations that if a small meander has sufficient amplitude and it can propagate eastward, the small meander grows locally and develops into a "large meander" upstream of the Izu Ridge, accompanying a stationary cyclonic eddy (e.g., Shoji 1972). Further, in a numerical experiment of the large meander using a two-layer model, Yoon and Yasuda (1987) have demonstrated that a solitary disturbance grows baroclinically if the initial amplitude is larger than a certain critical value. The present model consistently describes the above features of observations and experiments as follows:

- We have obtained two stable states, $a = a_+$ and 0, which can correspond to the large meander and the straight path, respectively. Further, when the solitary wave attains the large amplitude state, it becomes almost stationary in our model if we set $U_2 = 0$. (Of course, topography will play a crucial role in the behavior of large stationary meanders.)
- A solitary disturbance grows and develops into large amplitude state if the initial disturbance has an amplitude $a > a_-$ and if it propagates downstream. It decays otherwise. Hence, small meanders that develop into large meanders are rare, even though we frequently observe the small meanders off Kyushu, especially in winter (e.g., Sekine and Toba 1981).
- From the sign of the nonlinear coefficient (2.13c), (2.15b) implies that in dimensional terms only a cyclonic solitary wave may form in this system, which also corresponds to the formation of the cyclonic eddy on the large meander.

Although our model is highly idealized, evaluation of typical values may be useful. If we assume $H_1 = 700$ m, $H_2 = 3500$ m, $g' = 2 \times 10^{-2}$ m s^{-2}, $f_0 = 7 \times 10^{-5}$ s^{-1}, $U_0 = 1.0$ m s^{-1}, and if we use the mean current profile (3.13) and the scaled depth ratio (3.14a,b), then $\varepsilon^2 = 1/3$, $L_0 = 53$ km, and $\lambda_d^* = 0.23$. To evaluate ε, we recall that the relation between the scaled and the dimensional depth ratios is given by $H_1/H_2 = \varepsilon^2\sigma^{-1}\kappa^*\lambda_d^*\gamma$, from (2.16), where $\sigma = 1$ for the Boussinesq approximation. Note that with these typical values and with the dimensional value of β, 2×10^{-11} m^{-1} s^{-1}, β' is about 0.05, which is a small value. Hence, the scaling of the potential vorticity gradients in section 2 is relevant for strong currents such as Kuroshio.

Now we evaluate time scales. Since a characteristic time scale for a KdV solitary wave is $T_s = \varepsilon^{-3}L_0U_0^{-1}\lambda_d^{*-1}$, we then obtain $T_s \approx 13.9$ days. For the particular mean current profile and the depth ratio, the time scale of baroclinic growth, T_B, is longer than T_s (see Fig. 1b), where the unit time corresponds to T_s), that is, typically $T_B \sim 100$ days. Therefore, T_B corresponds well with the transition time of three to four months from observations. On the other hand, a barotropic decay time may be evaluated from $f_0\delta_E/2(H_1 + H_2)$, where δ_E is the bottom Ekman layer thickness. If we adopt $\delta_E = 10$ m, the typical time scale is about 130 days. A corresponding baroclinic decay time is ambiguous, but it should be longer than the barotropic decay time. A data analysis of Sekine et al. (1984) suggested that the spindown time of the cyclonic eddy on the large meander is about one year. Therefore, the time scale of baroclinic energy conversion is comparable to, but apparently exceeds, frictional dissipation. We conclude that the condition for baroclinic instability and multiple equilibria, such as (4.21), can be satisfied in practice.

One of the main results of this paper is that both bottom and interfacial friction are necessary for a two-layer model to have multiple stable equilibria (although a_+ may be unstable and show oscillatory behavior) because otherwise friction is destabilizing rather than stabilizing. However, the cause of interfacial friction is somewhat unclear, especially for oceanic phenomena. An important factor is radiation due to Rossby waves toward the ocean interior. Kubokawa (1989) considered it by introducing radiation in the lower layer, but for the upper layer he derived a KdV-type equation, so that radiative damping is not included there. He found that solitary waves are generated one after another, which tend to be stationary due to the lower-layer radiation. This is comparable to our result of the case of bottom friction only. If radiative damping is included in the upper-layer motion, then it may be described by an evolution equation of the Benjamin–Davis–Acrivos type (e.g., see Mitsudera and Grimshaw 1991b). Another factor to be noted is the possibility of continuous stratification in the lower layer because, in conjunction with the β effect, this permits transmission of energy downward, where it can be dissipated by bottom friction. As for baroclinic instability problems, bottom friction destabilizes the otherwise neutral Eady modes where $\beta = 0$ (e.g., Williams and Robinson

1974), whereas it invariably stabilizes Charney modes where $\beta \neq 0$ (e.g., Card and Barcilon 1982). Both these effects are important, and further investigation is needed.

Discussions developed here may be suggestive of the dynamics of blocking phenomena in the atmosphere as well. Recent observations suggest that blocking is a local phenomenon rather than a global one, and hence substantial modeling efforts have been made to explore *barotropic* solitary waves (e.g., Haines and Malanotte-Rizzoli 1991, and references therein). However, baroclinic processes may play important roles during the formation stage of blocks (e.g., Nakamura and Wallace 1990). Further, some blocking ridges show baroclinic features even during the fully developed stage. For example, Hartman and Ghan (1980) have shown that the temperature maximum of the long-lived Atlantic blocking ridges shifts westward from the center of the ridges, and hence there is net heat transport to the north. As for the Southern Hemisphere, Baines (1983) suggested that baroclinic instability is the most promising mechanism to form blocking in the Australian region where blocking events occur most frequently. Although the mechanism of blocking may be more complicated, and may involve barotropic processes such as barotropic instability and an eddy-straining mechanism (e.g., Mak 1991), the present model of localized baroclinic instability may shed light on the basic dynamics of blocking phenomena, in particular during their formation stage.

There is no doubt that forcing due to topographic features plays a crucial role in the evolution of localized phenomena such as atmospheric blocking and the Kuroshio large meander, especially influencing its stationary nature. Hence, a lot of studies have been carried out on these subjects. In the context of localized forcing, Warn and Brasnett (1983) have shown that a localized topography may capture a solitary disturbance propagating on a stable current if bottom friction is present. Yamagata and Umatani (1987) applied the mechanism to the bimodality of the Kuroshio paths. However, interaction between baroclinic currents and localized topography in the presence of friction has yet to be investigated. Finally, there is also a need to develop numerical and laboratory models that can examine the range of validity or robustness of the KdV dynamics, which assumes small amplitude and weak dispersion.

Acknowledgments. We would like to thank Drs. P. G. Baines and M. S. Borgas for critical reading of the manuscript. Comments of anonymous reviewers were also appreciated. One of us (HM) acknowledges support from ARC and Shell Australia.

APPENDIX

Energetic Considerations

Here we examine the energetics of the instability processes investigated in section 4. First, to obtain an energy equation we multiply (2.17b) by A and integrate with respect to X over $-\infty < X < \infty$ to get

$$-\left(\frac{\partial}{\partial T} + 2r_1\right)\int_{-\infty}^{\infty} \frac{1}{2}A^2 dX + \int_{-\infty}^{\infty} P_X A dX = 0, \quad \text{(A1a)}$$

where

$$P = \int_{-L}^{0} \psi U_1 dy. \quad \text{(A1b)}$$

Note that the second term in (A1a) shows that for upper-layer instability there must be a phase difference between the layers, with the phase of the lower layer farther downstream than that of the upper layer. To obtain a corresponding equation for the lower layer we first define Ψ and F by

$$\left(\frac{\partial}{\partial T} + U_2\frac{\partial}{\partial X} + \gamma r_2\right)\Psi = \psi, \quad \text{(A2a)}$$

and

$$\left(\frac{\partial}{\partial T} + U_2\frac{\partial}{\partial X} + \gamma r_2\right)F = \gamma A(\gamma r_2 U_1 + \nu r_1 U_{1yy}). \quad \text{(A2b)}$$

Then we can integrate (2.17b) with respect to T, multiply by ψ_X, and integrate with respect to y over $-L < y < 0$ and with respect to X over $-\infty < X < \infty$ to get

$$\gamma\int_{-\infty}^{\infty} P_X A dX + \left(\frac{\partial}{\partial \tau} + 2\gamma r_2\right)\int_{-\infty}^{\infty} J dX = -\gamma\int_{-\infty}^{\infty} AG dX, \quad \text{(A3a)}$$

where

$$J = \frac{1}{2}\int_{-L}^{0} Q_{2y}\Psi_X^2 dy - \int_{-L}^{0} F\Psi_X dy, \quad \text{(A3b)}$$

and

$$G = \int_{-L}^{0} \Psi_X(\gamma r_2 U_1 + \nu r_1 U_{1yy}) dy. \quad \text{(A3c)}$$

Combining (A1a) and (A3a) we get the energy equation

$$\left(\frac{\partial}{\partial T} + 2r_1\right)\int_{-\infty}^{\infty}\frac{1}{2}A^2 dX + \gamma^{-1}\left(\frac{\partial}{\partial T} + 2r_2\right) \times \int_{-\infty}^{\infty} J dX = -\int_{-\infty}^{\infty} AG dX. \quad \text{(A4)}$$

In the absence of friction (i.e., $r_1 = r_2 = 0$) it reduces to the result obtained by MG, which shows that for $J < 0$ there is instability. Here, in the absence of friction $F = G = 0$, and so $J < 0$ is possible only if $Q_{2y} < 0$ somewhere, which is the well-known necessary condition for baroclinic instability. Here interest is in the

role of the frictional terms, and we see from (A3a–c) and (A4) that frictional terms first modify the time-derivative term on the left-hand side of (A4) in an obvious way; second, they alter the definition of J; and third, they introduce a term on the right-hand side of (A4). Of these, the most important is the term involving G. Note that for the jetlike flows considered here $U_1 > 0$ and $U_{1yy} < 0$ so that interfacial friction (represented by r_1) and bottom friction (represented by r_2) act in opposite senses.

In general, the sign of the right-hand side of (A4) cannot easily be determined, and hence to make progress we resort to perturbation theory. As in the preceding parts of this section we assume that $\gamma \ll 1$, but first we consider nonresonant coupling between the layers. In this situation the slow time variable is

$$\tau = \gamma T, \tag{A5}$$

in place of (4.1), and we replace r_1 with γr_1 so that bottom and interfacial frictional terms are comparable with time scales in sympathy with τ. With these scalings F is $O(\gamma^2)$ and it turns out that its contribution to J (A3b) can be neglected.

Let us first consider the U mode, for which we can write

$$A = A^{(0)} + \gamma A^{(1)} + \cdots, \tag{A6a}$$

$$\psi = \gamma \psi^{(0)} + \cdots. \tag{A6b}$$

Then $A^{(0)}$ satisfies the uncoupled equation. Further,

$$J = \gamma^2 J^{(0)} + \cdots, \tag{A7a}$$

where

$$J^{(0)} = \frac{1}{2}\int_{-L}^{0} Q_{2y}\Psi_X^{(0)2} dX, \tag{A7b}$$

and, to leading order, the energy equation (A4) becomes

$$\left(\frac{\partial}{\partial\tau} + 2r_1\right)\int_{-\infty}^{\infty}\frac{1}{2}A^{(0)2}dX + \gamma\left(\frac{\partial}{\partial\tau} + 2r_2\right)\int_{-\infty}^{\infty} J^{(0)}dX = -\gamma\int_{-\infty}^{\infty} A^{(0)}G^{(0)}dX, \tag{A8a}$$

where

$$G^{(0)} = \int_{-L}^{0}\Psi_X^{(0)}(r_2U_1 + \nu r_1 U_{1yy})dy. \tag{A8b}$$

Thus, to leading order, the energy density is dominated by the upper-layer solution, and we can neglect the term involving $J^{(0)}$ on the left-hand side of (A8a), as well as the right-hand side. Hence to leading order the upper-layer solution is stable. However, we can examine these neglected terms to determine whether or not their tendency is to destabilize the upper-layer motion. First we consider the term involving $J^{(0)}$ on the left-hand side of (A8a) and note that if $Q_{2y} < 0$, this term is destabilizing if $r_2 \gg r_1$. Next, to estimate the sign of the right-hand side of (A8a), we suppose that

$$\psi^{(0)} = \sum_{n=1}^{\infty} B_n(X, T)(U_2 - q_n)\eta_n(y), \tag{A9}$$

where $\eta_n(y)$ satisfies the eigenvalue problem (3.2a,b). For simplicity we suppose that U_2 is a constant. Then substituting (A6a,b) and (A9) into (2.17b,c), and assuming that $A^{(0)}$ is a solitary wave of speed c, it is readily shown that

$$\Psi_X^{(0)} = \psi^{(0)}/(U_2 - c), \tag{A10a}$$

and

$$B_n = \frac{(U_2 - c)\displaystyle\int_{-L}^{0} U_1\eta_n dy}{(q_n - c)\displaystyle\int_{-L}^{0} Q_{2y}\eta_n^2 dy}A^{(0)}. \tag{A10b}$$

Then we find that

$$\int_{-\infty}^{\infty} A^{(0)}G^{(0)}dX = \int_{-\infty}^{\infty} A^{(0)2}dX\left[\sum_{n=1}^{\infty}\frac{(U_2 - q_n)}{(q_n - c)}G_n\right], \tag{A11a}$$

where

$$\left[\int_{-L}^{0} Q_{2y}\eta_n^2 dy\right]G_n = \int_{-L}^{0} U_1\eta_n dy \times\left(r_2\int_{-L}^{0} U_1\eta_n dy + \nu r_1\int_{-L}^{0} U_{1yy}\eta_n dy\right). \tag{A11b}$$

Since we can expect $Q_{2y}(U_2 - q_n) > 0$, while $U_1 > 0$ and $U_{1yy} < 0$ for jetlike flows, it follows that the right-hand side of (A8a) is destabilizing if $r_2 \gg r_1$ and $c > q_n$, or if $r_1 \gg r_2$ and $c > q_n$. In both cases we again see that friction can be destabilizing.

Next we consider the L mode, for which

$$A = A^{(0)} + \gamma A^{(1)} + \cdots, \tag{A12a}$$

$$\psi = \psi^{(0)} + \gamma\psi^{(1)} + \cdots, \tag{A12b}$$

where $\psi^{(0)}$ is again given by (A9). However, now the $\psi^{(0)}$ is uncoupled from $A^{(0)}$, and hence we are free to select a single mode, say $n = N$. To leading order, the energy equation is

$$\left(\frac{\partial}{\partial\tau} + 2r_1\right)\int_{-\infty}^{\infty}\frac{1}{2}A^{(0)2}dX + \gamma^{-1}\left(\frac{\partial}{\partial\tau} + 2r_2\right)\int_{-\infty}^{\infty} J^{(0)}dX = -\int_{-\infty}^{\infty} A^{(0)}G^{(0)}dX, \tag{A13a}$$

where

$$J^{(0)} = \frac{1}{2}\left(\int_{-L}^{0} Q_{2y}\eta_N^2 dy\right)B_N^2, \qquad \text{(A13b)}$$

and

$$G^{(0)} = B_N \int_{-L}^{0} \eta_N(\gamma r_2 U_1 + \nu r_1 U_{1yy})dy. \qquad \text{(A13c)}$$

Thus, to leading order, the energy density is dominated by the lower-layer solution and is positive or negative according as $Q_{2y} > 0$ or < 0. It follows that the term involving the upper-layer motion on the left-hand side of (A13a) is destabilizing if $r_2 \gg r_1$ and $Q_{2y} < 0$. To estimate the sign of the right-hand side of (A13a) we must find $A^{(0)}$, which is given by

$$-(\Delta - q_N)A^{(0)} + 3A^{(0)2} + A_{XX}^{(0)} + B_N\left[\int_{-L}^{0}(U_2 - q_N)U_1\eta_N dy\right] = 0. \qquad \text{(A14)}$$

Using the linear, nondispersive limit, we finally estimate that

$$\int_{-\infty}^{\infty} A^{(0)}G^{(0)}dX = \int_{-\infty}^{\infty} B_N^2 dX\left[\frac{(U_2 - q_N)G_1}{\Delta - q_N}\right], \qquad \text{(A15)}$$

where G_1 is given by (A11b). It follows that the right-hand side of (A13a) is destabilizing if $r_2 \gg r_1$ and $\Delta < q_N$, or if $r_1 \gg r_2$ and $\Delta > q_N$. Again we see that friction can be destabilizing.

Finally we reexamine the resonant case discussed in detail in the previous subsections. Now the slow time variable is (4.1), ψ is given by (4.2), and $A = A_s + O(\gamma^{1/2})$, where A_s is the solitary wave solution given by (4.4a–c). To leading order, the energy equation (A4) becomes

$$\left(\frac{\partial}{\partial\tau} + 2r_1\right)\int_{-\infty}^{\infty}\frac{1}{2}A_s^2 dX + \left(\frac{\partial}{\partial\tau} + 2r_2\right)\frac{1}{b}\int_{-\infty}^{\infty}\frac{1}{2}B^2 dX = -\gamma^{1/2}2lI_B \times\left(r_1 + \nu r_1\frac{\int_{-\infty}^{\infty}U_{1yy}\eta_N dy}{\int_{-L}^{0}U_1\eta_1 dy}\right). \qquad \text{(A16)}$$

Here, we recall that $\psi^{(0)}$ is given by (4.8), b is defined by (3.6d), and I_B is given by (4.5c). Note that now the upper and lower layers contribute equally to the energy density. It is interesting to note here that (A1a) gives, to leading order,

$$\left(\frac{\partial}{\partial\tau} + 2r_1\right)\int_{-\infty}^{\infty}\frac{1}{2}A_s^2 dX = 2lI_B. \qquad \text{(A17)}$$

Evaluating the integral on the left-hand side, we find that (A17) gives (4.5a). Also (A3a) gives, to leading order,

$$\left(\frac{\partial}{\partial\tau} + 2r_2\right)\int_{-\infty}^{\infty}\frac{1}{2}B^2 dX + 2blI_B = 0. \qquad \text{(A18)}$$

Eliminating I_B gives (A16) with the right-hand side replaced with zero, which is, of course, the correct result to O(1). Thus we see that (A16) gives an $O(\gamma^{1/2})$ correction term to the perturbation theory of the previous three subsections. We conclude, for instance, that if $b > 0$, so that the solitary wave is stable to leading order, the right-hand side of (A16) is destabilizing if $r_2 \gg r_1$. However, when $b < 0$ it is difficult to draw general conclusions from (A16) since the sign of the energy density on the left-hand side of (A16) is not known a priori. However, we should note here that the second perturbation equation (4.5b) is not included in the set (A16), (A17), or (A18) but is obtained as an $O(\gamma^{1/2})$ correction term from the energy equation (A1a), where (A17) is the leading-order term (see Grimshaw and Mitsudera 1992).

REFERENCES

Baines, P. G., 1983: A survey of blocking mechanisms, with application to the Australian region. *Aust. Meteor. Mag.*, **31**, 27–36.

Card, P. A., and A. Barcilon, 1982: The Charney stability problem with a lower Ekman layer. *J. Atmos. Sci.*, **39**, 2128–2137.

Drazin, P., and W. Reid, 1981: *Hydrodynamic Stability*. Cambridge University Press, 525 pp.

Fornberg, B., and G. B. Whitham, 1978: A numerical and theoretical study of certain nonlinear phenomena. *Phil. Trans. Roy. Soc.*, **A289**, 373–404.

Grimshaw, R., 1979: Slowly varying solitary waves. I. Kortweg-de Vries equation. *Proc. Roy. Soc. London*, **A368**, 359–375.

———, and J. S. Allen, 1982: The effect of dissipation on linearly coupled, slowly varying oscillators. *Stud. Appl. Math.*, **67**, 169–198.

———, and H. Mitsudera, 1992: Slowly-varying solitary wave solutions of the perturbed Korteweg-de Vries equation revisited. *Stud. Appl. Math.*, in press.

Haines, K., and P. Malanotte-Rizzoli, 1991: Isolated anomalies in westerly jet streams: A unified approach. *J. Atmos. Sci.*, **48**, 510–526.

Hartman, D. L., and S. J. Ghan, 1980: A statistical study of the dynamics of blocking. *Mon. Wea. Rev.*, **108**, 1144–1159.

Holopainen, E., 1961: On the effect of friction on baroclinic waves. *Tellus*, **13**, 363–367.

Karpman, V. I., and E. M. Maslov, 1978: Structure of tails under the action of perturbation on solitons. *Sov. Phys. JETP*, **48**, 252–259.

Kaup, D. J., and A. C. Newell, 1978: Solitons as particles and oscillators and in slowly varying media: a singular perturbation theory. *Proc. Roy. Soc. London*, **A361**, 413–446.

Kodama, Y., and M. J. Albowitz, 1981: Perturbation of soliton and solitary waves. *Stud. Appl. Math.*, **64**, 225–245.

Kubokawa, A., 1988: Instability and nonlinear evolution of a density driven coastal current with a surface front in a two-layer ocean. *Geophys. Astrophys. Fluid Dyn.*, **40**, 195–223.

———, 1989: Growing solitary disturbance in a baroclinic boundary current. *J. Phys. Oceanogr.*, **19**, 182–192.

Mak, M., 1991: Dynamics of an atmospheric blocking as deduced

from its local energetics. *Quart. Roy. Meteor. Soc.*, **117,** 477–493.

Merkine, L.-O., 1977: Convective and absolute instability of baroclinic eddies. *Geophys. Astrophys. Fluid Dyn.*, **9,** 129–157.

Mitsudera, H., and K. Hanawa, 1989: Frictional coastal trapped waves in two-layered ocean. *J. Fluid Mech.*, **198,** 453–469.

———, and R. Grimshaw, 1991a: Generation of mesoscale variability by resonant interaction between a baroclinic current and localized topography. *J. Phys. Oceanogr.*, **21,** 737–765.

———, and R. Grimshaw, 1991b: Effects of radiative damping on resonantly generated internal gravity waves. *Stud. Appl. Math.*, **84,** 183–206.

Nakamura, H., and J. M. Wallace, 1990: Observed changes in baroclinic wave activity during the life cycle of low-frequency circulation anomalies. *J. Atmos. Sci.*, **47,** 1100–1116.

Pedlosky, J., 1989: Simple model for local instabilities in zonally inhomogeneous flows. *J. Atmos Sci.*, **46,** 1769–1778.

———, 1992: Baroclinic instability localized by dissipation. *J. Atmos. Sci.*, **49,** 1161–1170.

———, and C. Frenzen, 1980: Chaotic and periodic behavior of finite-amplitude baroclinic waves. *J. Atmos. Sci.*, **37,** 631–647.

Samelson, R. M., and J. Pedlosky, 1990: Local baroclinic instability of flow over variable topography. *J. Fluid Mech.*, **221,** 411–456.

Sekine, Y., and Y. Toba, 1981: Velocity variation of the Kuroshio during formation of the small meander. *J. Oceanogr. Soc. Japan,* **37,** 87–93.

———, H. Ishii, and Y. Toba, 1984: Spin-up and spin-down processes of the large cold water mass of the Kuroshio south of Japan. *J. Oceanogr. Soc. Japan,* **41,** 207–212.

Shoji, D., 1972: The variation of the Kuroshio south of Japan. *Kuroshio: Its Physical Aspects,* H. Stommel and K. Yoshida, Eds., University of Tokyo Press, 227–234.

Warn, T., and B. Brasnett, 1983: The amplification and capture of atmospheric solitons by topography: A theory of the onset of regional blocking. *J. Atmos. Sci.*, **40,** 28–38.

Williams, G. P., and J. B. Robinson, 1974: Generalized Eady waves with Ekman pumping. *J. Atmos. Sci.*, **31,** 1768–1776.

Yamagata, T., and S. Umatani, 1987: The capture of current meander by coastal geometry with possible application to the Kuroshio Current. *Tellus,* **39A,** 161–169.

Yoon, J. H., and I. Yasuda, 1987: Dynamics of Kuroshio meander: Two-layer model. *J. Phys. Oceanogr.*, **17,** 66–81.